Supplement to: *Agricultural breadbaskets shift poleward given adaptive farmer behavior under climate change*

James A. Franke[1,2], Christoph Müller[3], Sara Minoli[3], Joshua Elliott[2], Christian Folberth[4], Charles Gardner[5], Tobias Hank[6], R. Cesar Izaurralde[7], Jonas Jägermeyr[8,3,9], Curtis D. Jones[7], Wenfeng Liu[10], Stefan Olin[11], Thomas A.M. Pugh[11,12,13], Alex C. Ruane[8], Haynes Stephens[1,2], Florian Zabel[6], and Elisabeth J. Moyer[1,2,*]

[1]*Department of the Geophysical Sciences, University of Chicago, Chicago, USA*
[2]*Center for Robust Decision-making on Climate and Energy Policy (RDCEP), University of Chicago, Chicago, USA*
[3]*Potsdam Institute for Climate Impacts Research (PIK), Member of the Leibniz Association, Potsdam, Germany*
[4]*Ecosystem Services and Management Program, International Institute for Applied Systems Analysis, Laxenburg, Austria*
[5]*Program on Global Environment, University of Chicago, Chicago, USA*
[6]*Ludwig-Maximilians-Universität München (LMU), Munich, Germany*
[7]*Department of Geographical Sciences, University of Maryland, College Park, MD, USA*
[8]*NASA Goddard Institute for Space Studies, New York, USA*
[9]*Columbia University Center for Climate Systems Research, New York, USA*
[10]*College of Water Resources and Civil Engineering, China Agricultural University, Beijing 100083, China*
[11]*Department of Physical Geography and Ecosystem Science, Lund University, Lund, Sweden*
[12]*School of Geography, Earth and Environmental Sciences, University of Birmingham, Birmingham, UK*
[13]*Birmingham Institute of Forest Research, University of Birmingham, Birmingham, UK*

Contents

# Additional scenarios simulated with LPJmL

In addition to the GGCMI Phase 2 data set, we ran the LPJmL model (von Bloh et al. 2018) for additional scenarios to allow for better analysis of the mechanisms that determine future spatial yield patterns under climate change. One important shortcoming of the GGCMI Phase 2 data set is that the only adaptation mechanism considered is the regaining of the growing season that shortens under warming due to accelerated phenological development (A1), while the adaptation in sowing dates is ignored in this data set. Also, regaining the growing season under warming must not necessarily be a useful adaptation measure, as shorter growing seasons could also be beneficial, e.g. to avoid terminal drought (Minoli et al. 2019b).

For the extra simulations, we do not reproduce the GGCMI experimental setup with regular disturbances of the historical AgMERRA climate data set along the T and W dimensions, but conduct simulations for transient climate projections from the ISIMIP2b project (Frieler et al. 2017), making use of bias corrected climate scenarios of HadGEM, MIROC, GFDL, and IPSL for the high-end radiative forcing scenario RCP8.5. For each of these climate scenarios, we developed adapted planting date and harvest date scenarios for the end of the 21st century, making use of the rule-based approach described by Minoli et al. (2019a) and Waha et al. (2012). These scenarios assume no delay in cultivar development, so that optimal growing seasons can be exploited with suitably fast/slow maturing cultivars.
Simulations were conducted for the period 1980-2099, covering the historical reference period (1980-2010) and the future period (2070-2099). For the historical period, we use rule-based rather than observed growing seasons (as done in the GGCMI Phase 2 experiment), to avoid comparing apples and oranges when comparing historical and future yield patterns. We conducted simulations where only the sowing dates (*planting advance*), only the cultivar (*maturity delay*) or both (*plant & maturity*) were adapted, in order to allow for separating the effects.

On top of these growing season adaptation scenarios, we conducted simulations with modified input data, where all gridcells were parameterized to have the soil properties as well as the same radiation inputs of Cedar Rapids, IA, USA. With this unrealistic simulation setup (*soils & rad.*), we intended to see if the remaining differences of yield levels with adapted growing seasons and shifted breadbasket locations could be explained by centrally important, but non-transferable properties. This setup is computed for non-adapted growing seasons as well as in combination with the full growing season adaptation (*plant & maturity*).
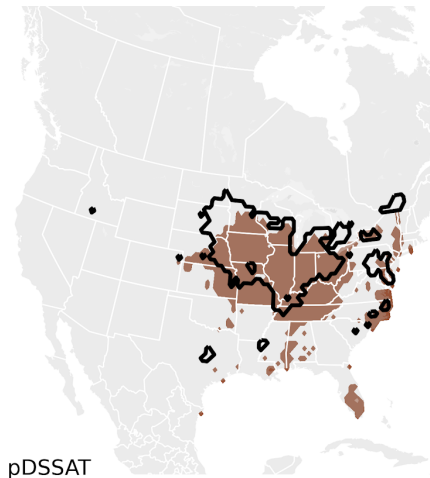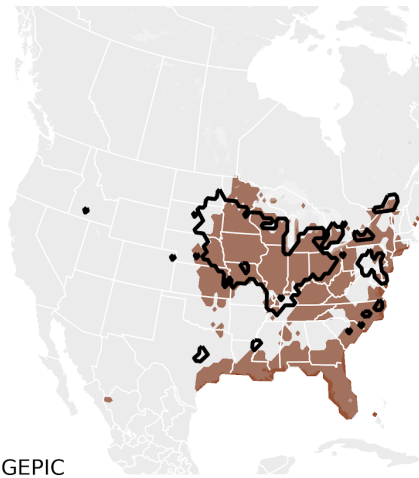
Supplementary Figures
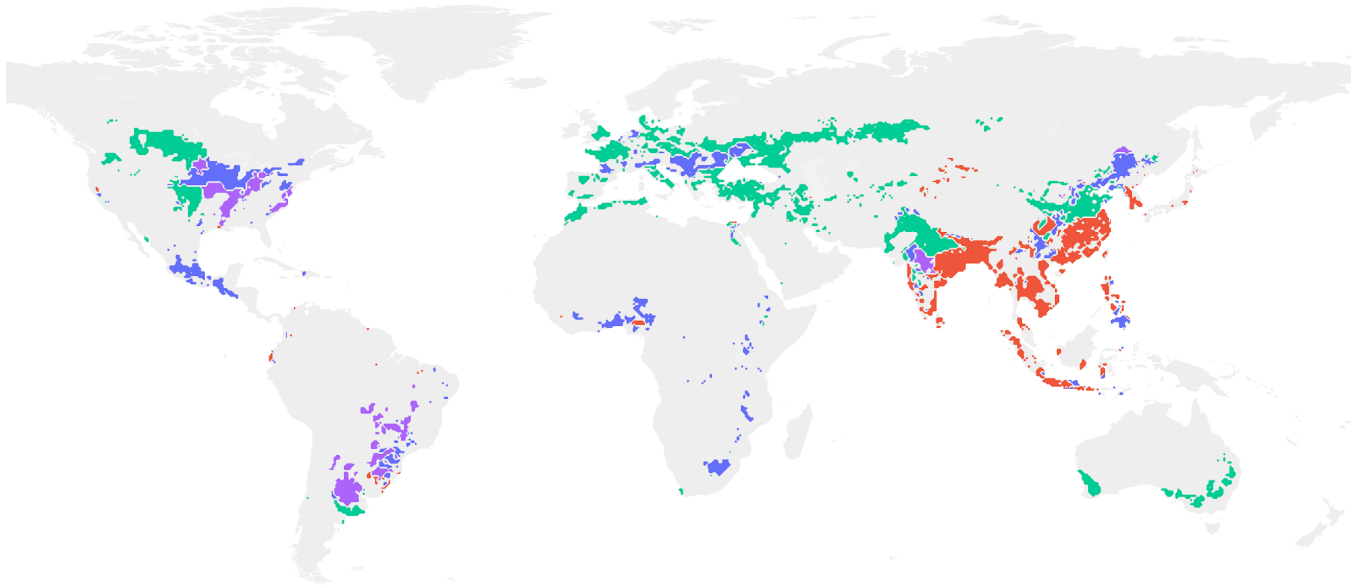
Supplemental Figure S1 | Major Breadbasket locations. Top 20% cultivation intensity regions globally for maize (blue), soybean (purple), wheat (green), and rice (red). Data from MIRCA2000 (Portmannn et al. 2010).
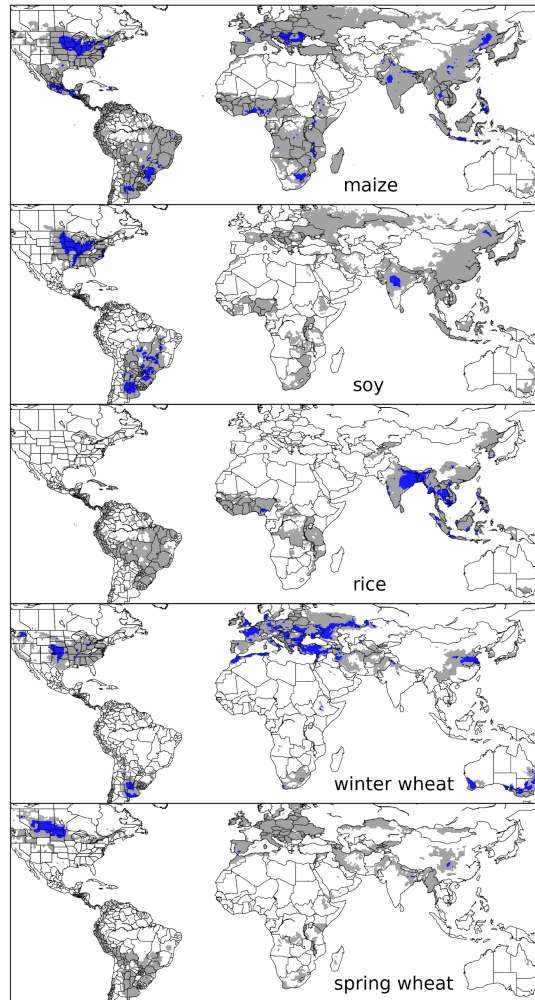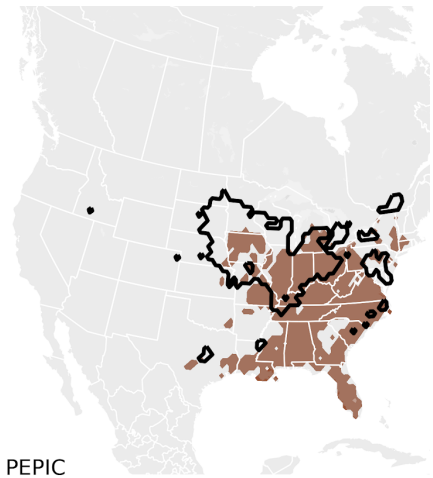
Figure S2 | Presently cultivated area for rainfed crops from MIRCA2000. Blue indicates grid cells with more that 20,000 hectares (~10% of the equatorial grid cell). Gray contour shows the area at least 10 hectares cultivated per grid cell. Data from MIRCA2000 (Portmannn et al. 2010).
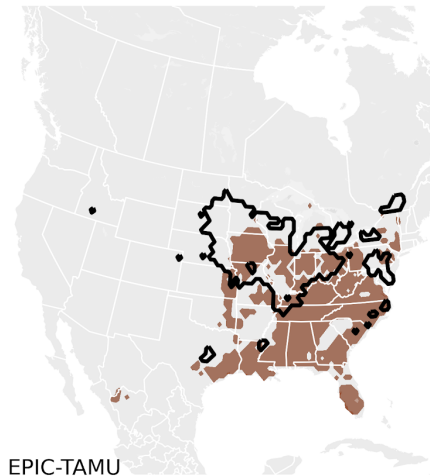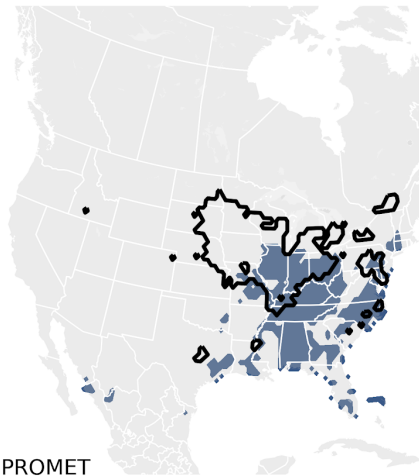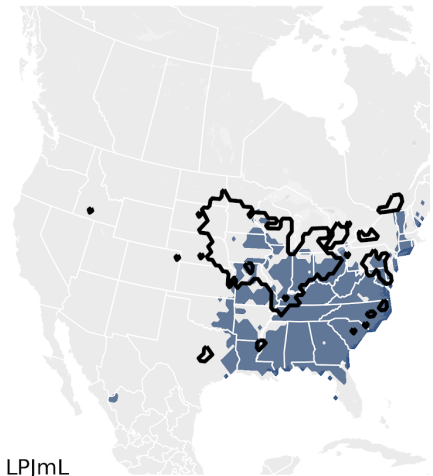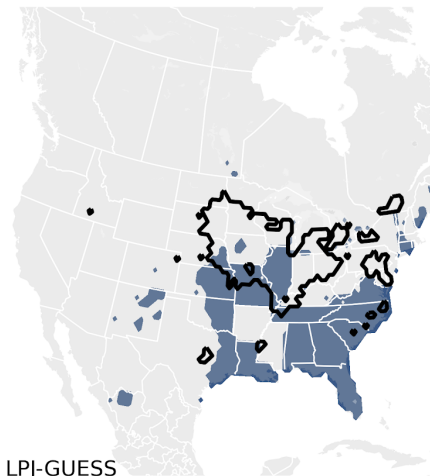
Supplemental Figure S3 | Ecosystem vs site based model comparison, historical simulations. Top 10% simulated grid cells in North America for each model for rainfed maize under historical conditions (1980-2010). Black contour is the top 15% rainfed cultivation intensity for reference. Site-based models generally do a better job of locating the best yields in the midwest corn belt, though all models other than pDSSAT place much of the best yields on the gulf coast.
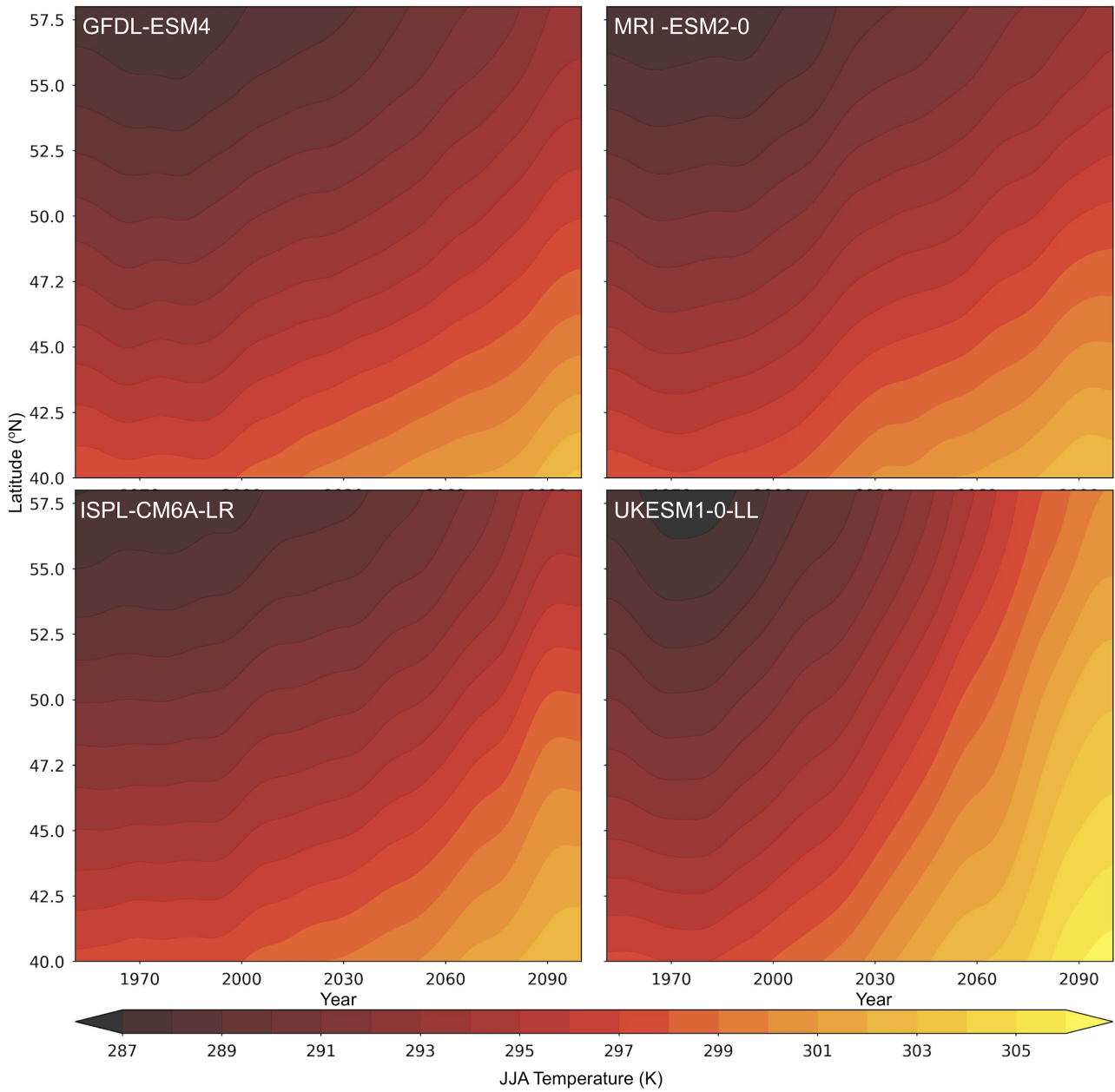
Supplemental Figure S4 | CMIP6 temperature shifts along latitudes (SSP585). June-July-August zonal mean temperature in North America (over only agricultural land) for select CMIP6 models for SSP585. Isotherms show poleward progression of growing season temperature analogue. Yearly temperatures smoothed with a gaussian filter to show climatology. Data from O'Neill et al. 2016.
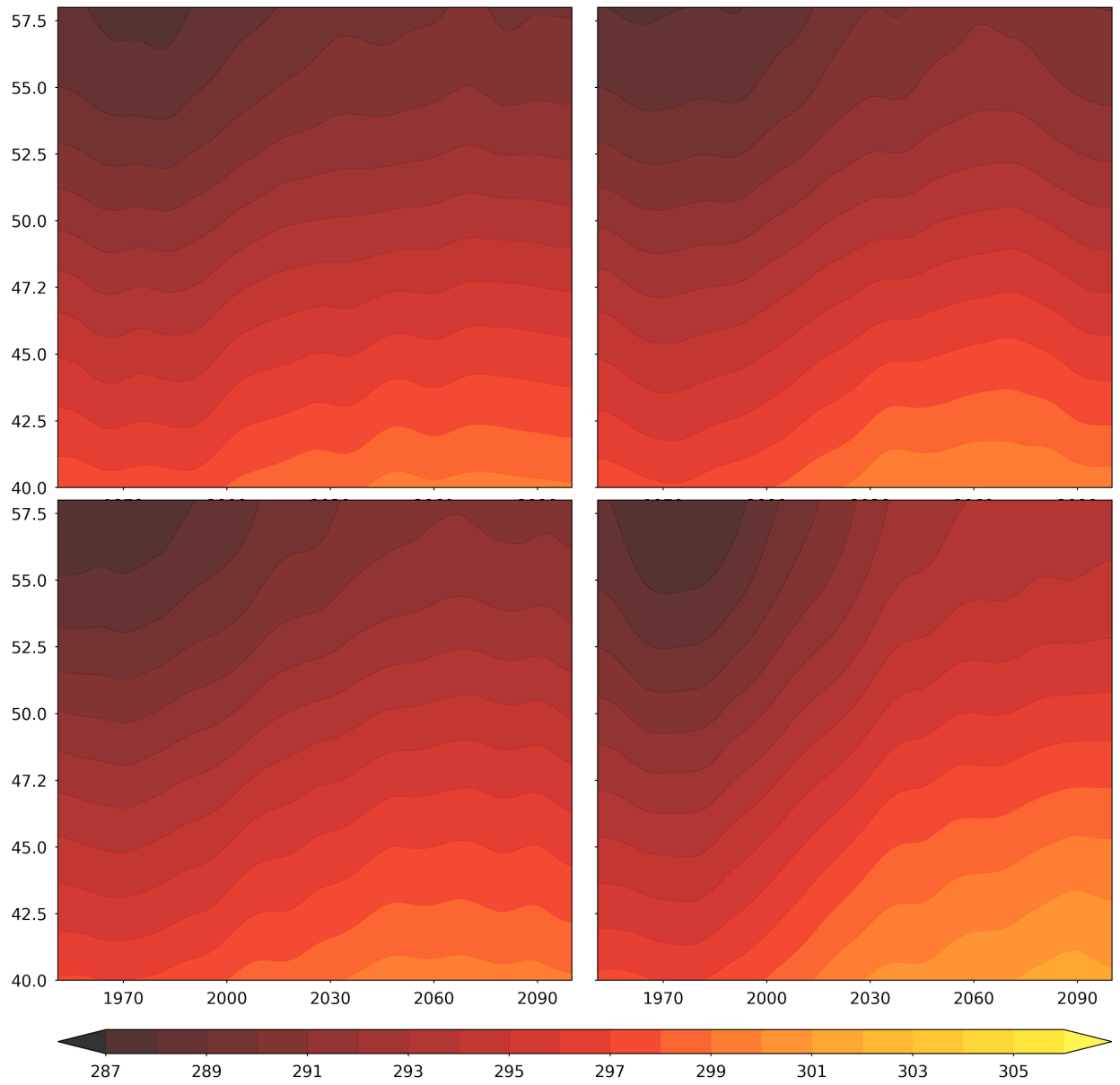
Supplemental Figure S5 | CMIP6 temperature shifts along latitudes (SSP126). Same as above, now for SSP126. UKESM (lower right quadrant, a high sensitivity model) shows 5°C of temperature rise at 42N (Cedar Rapids).
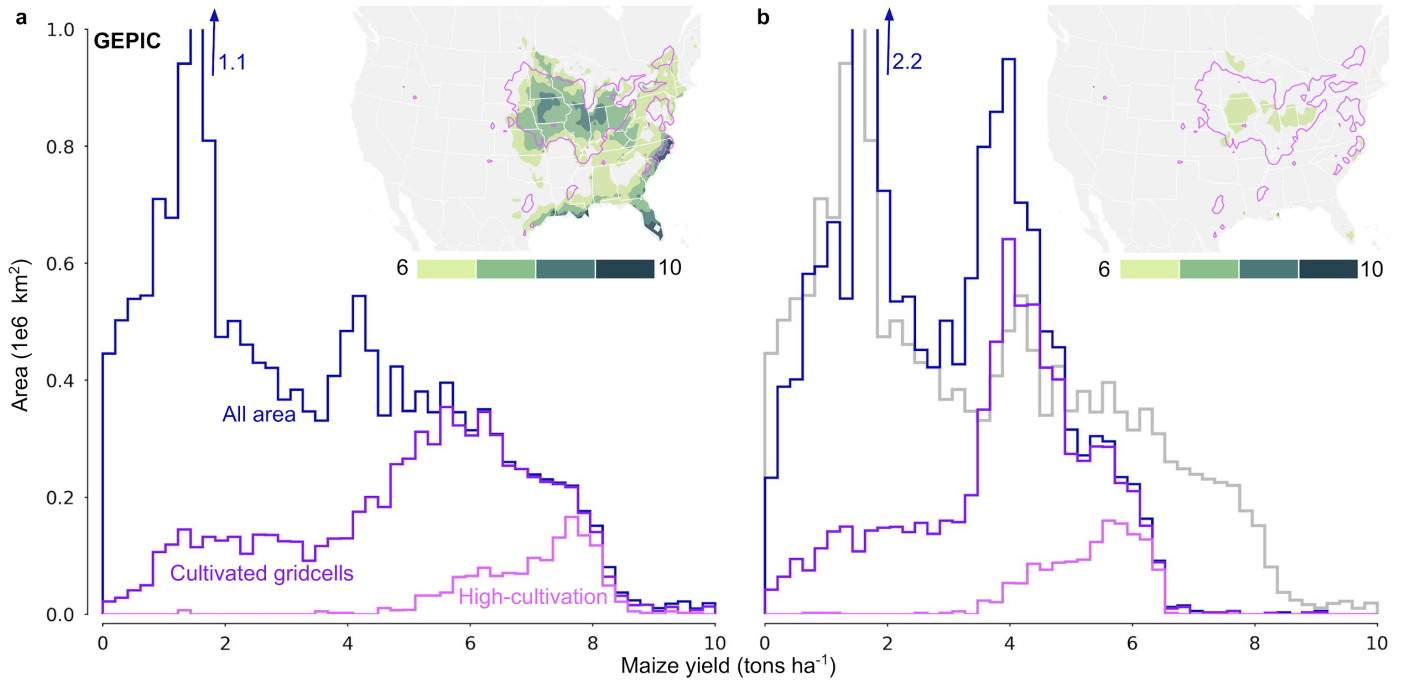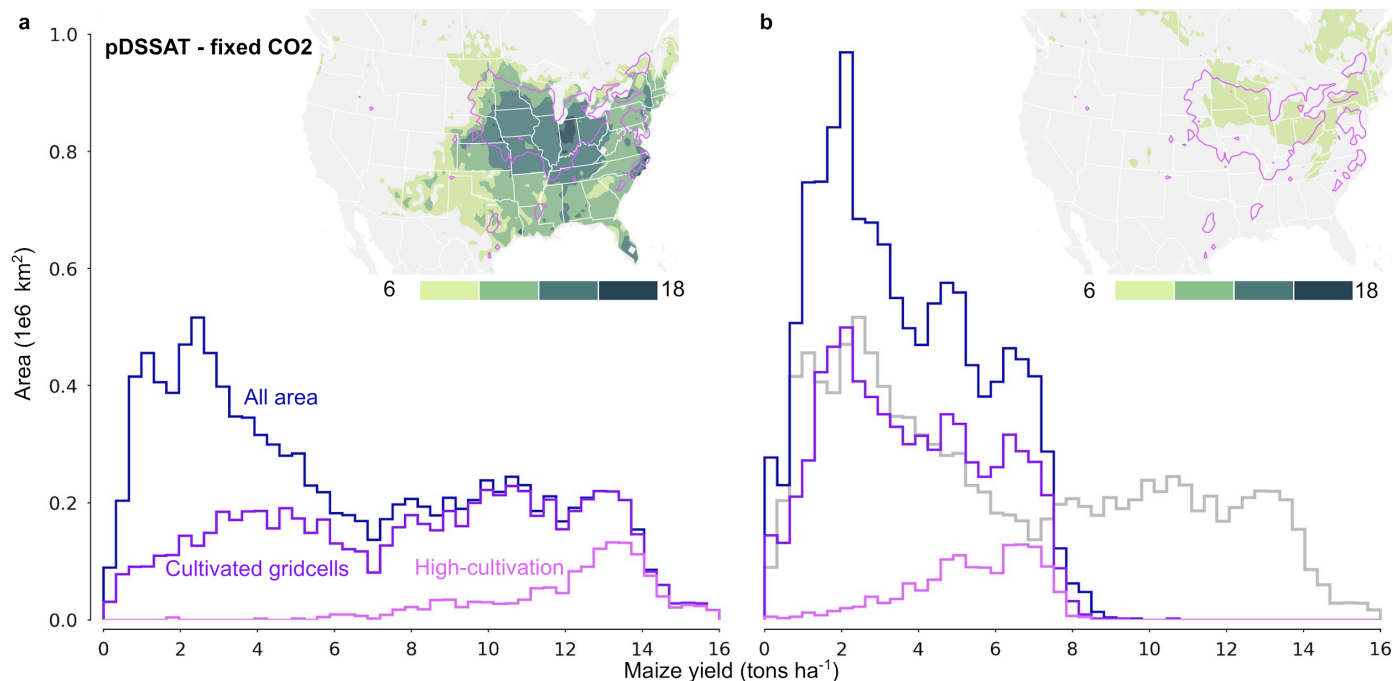
Supplemental Figure S6 | Same convention as main text Figure 2, except now for high [CO_2] of 810 ppm from the GEPIC model. Simulations are the A0 growing season specification.
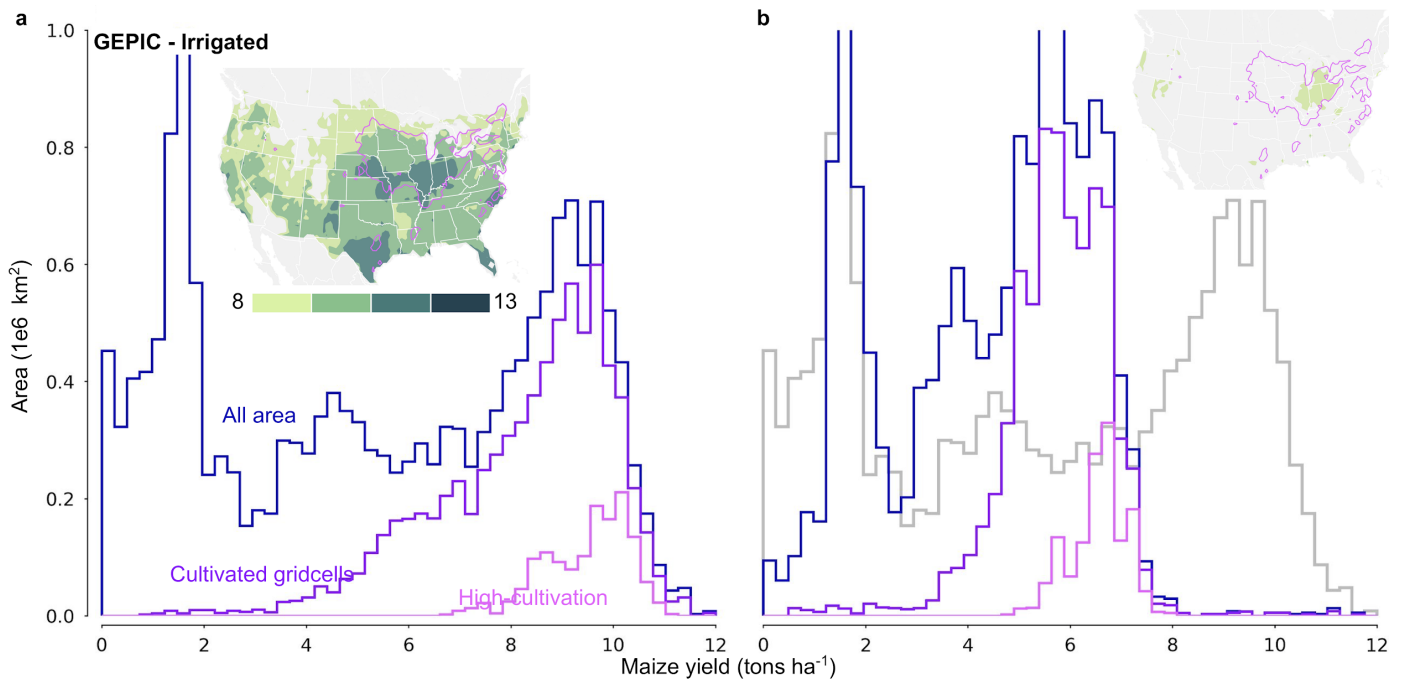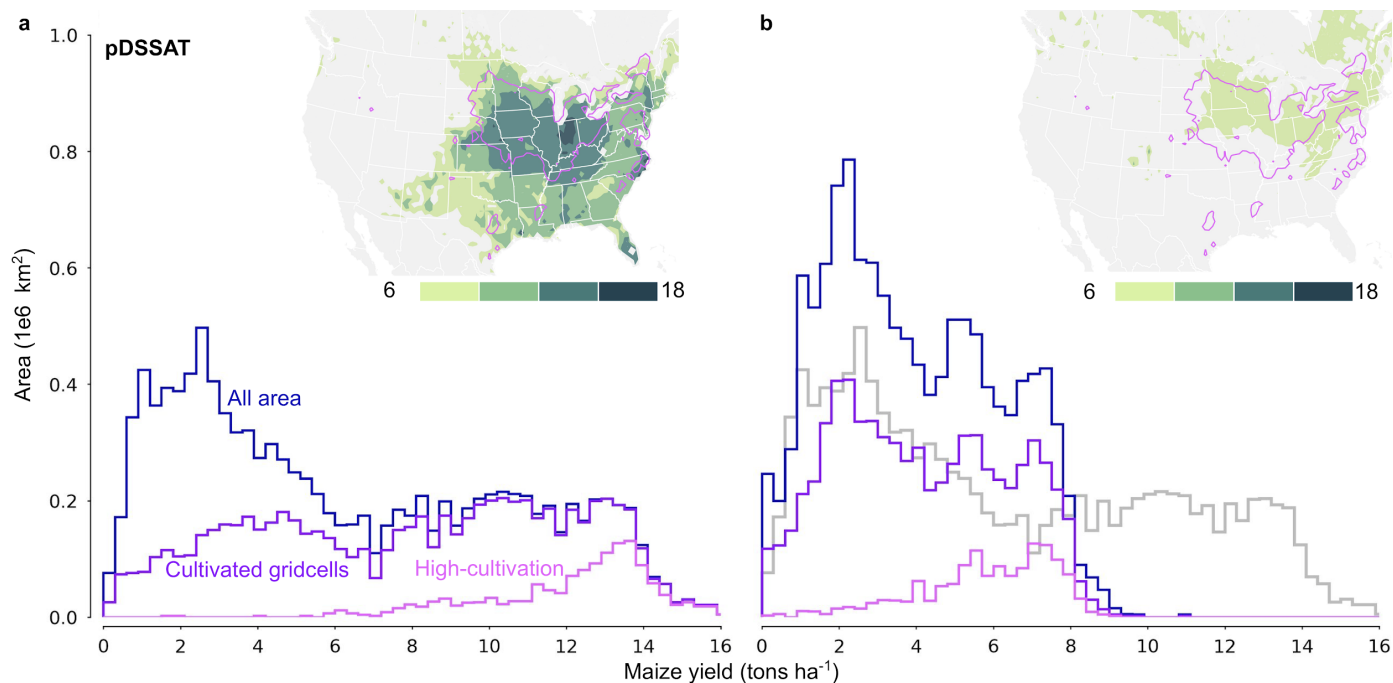

Supplemental Figure S7 | Same convention as main text Figure 2, except now for **irrigated** simulations from the GEPIC model. Simulations are the A0 growing season specification.
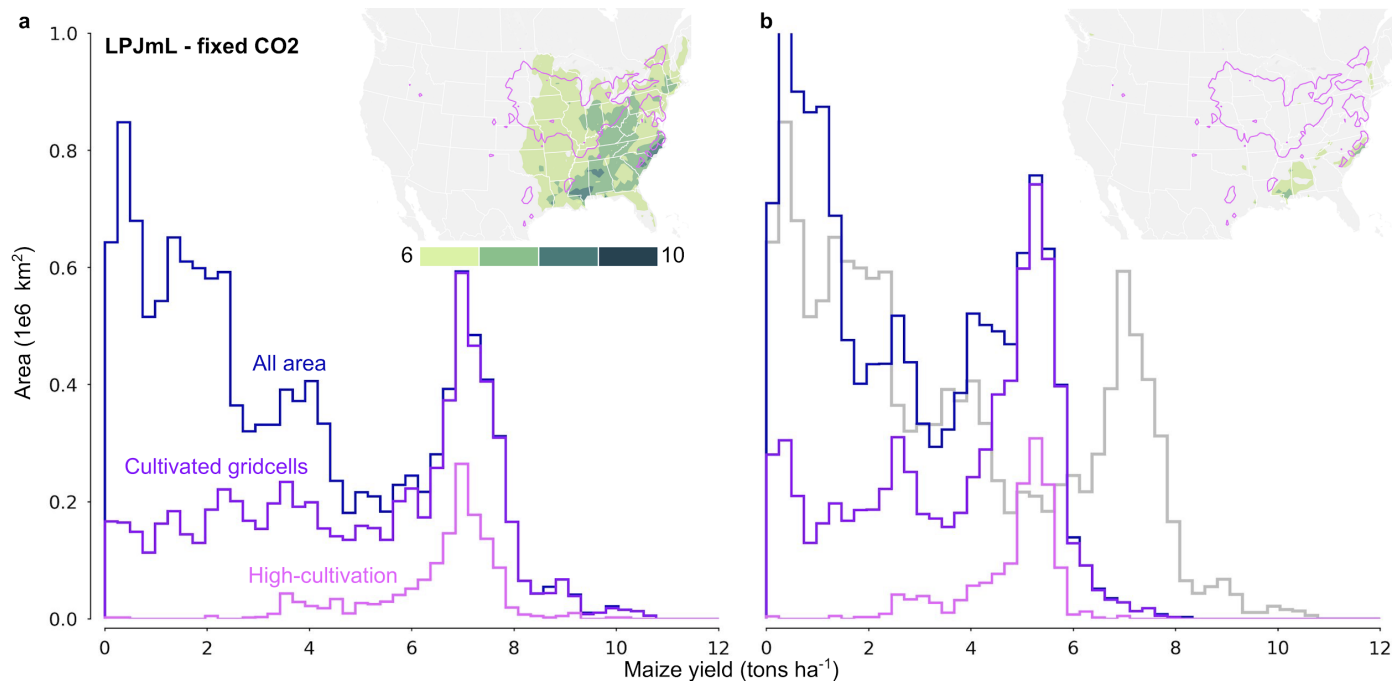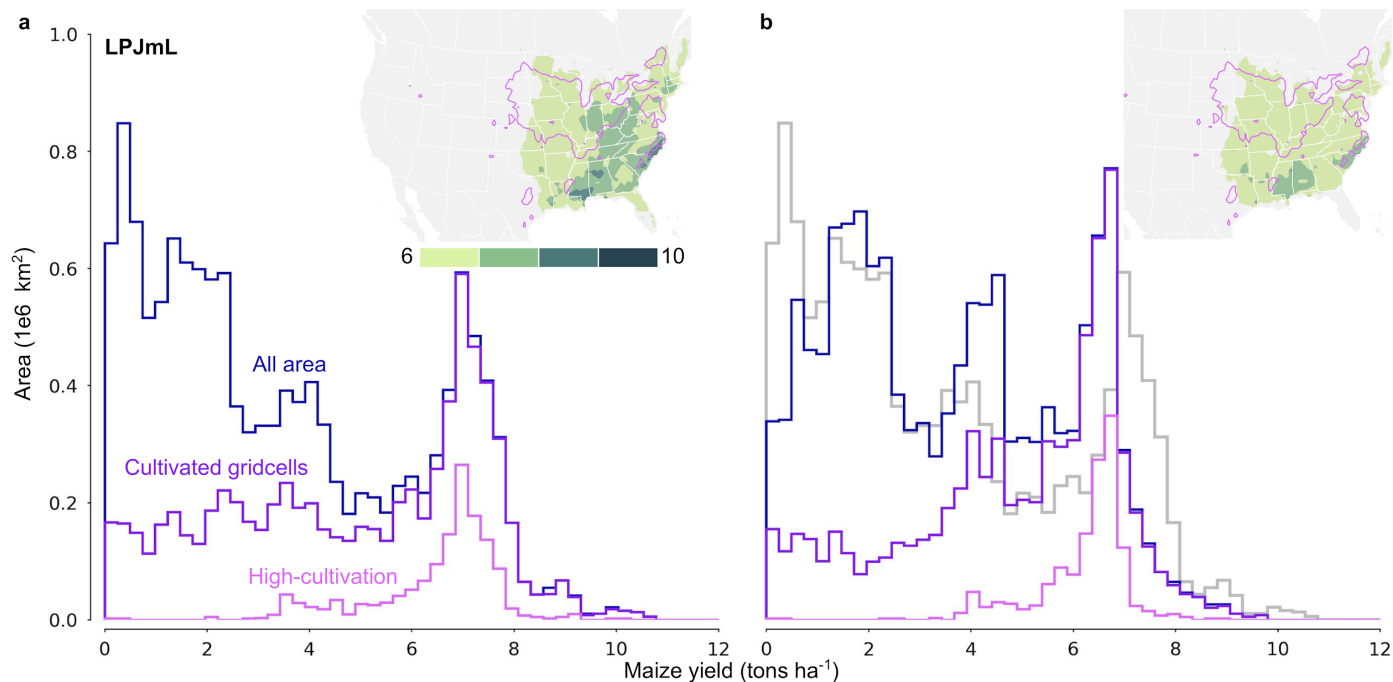
Supplemental Figure S8 | Same convention as main text Figure 2, except now for the pDSSAT model. Simulations are the A0 growing season specification.

Supplemental Figure S9 | Same convention as main text Figure 2, except now for the pDSSAT model with high [CO_2] of 810 ppm. Simulations are the A0 growing season specification.

Supplemental Figure S10 | Same convention as main text Figure 2, except now for LPJmL (**GGCMI Phase 2**). Simulations are the A0 growing season specification.

Supplemental Figure S11 | Same convention as main text Figure 2, except now for LPJmL (**GGCMI Phase 2**) with high [CO_2] of 810 ppm. Simulations are the A0 growing season specification.

Supplemental Figure S12 | Same convention as main text Figure 2, except now for PEPIC. Simulations are the A0 growing season specification.
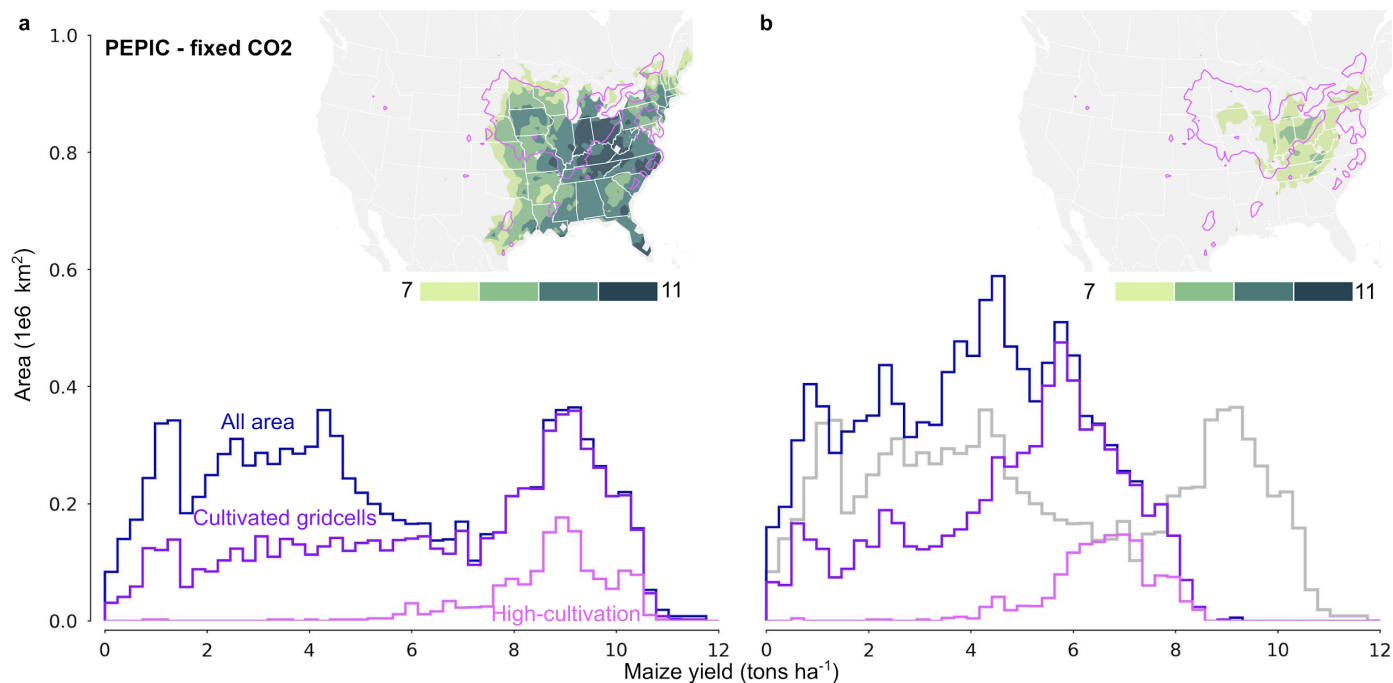

Supplemental Figure S13 | Same convention as main text Figure 2, except now for PEPIC with high [CO$_2$] of 810 ppm. Simulations are the A0 growing season specification.

Supplemental Figure S14 | Same convention as main text Figure 2, except now for EPIC-TAMU. Simulations are the A0 growing season specification.

Supplemental Figure S15 | Same convention as main text Figure 2, except now for EPIC-TAMU with high [CO_2] of 810 ppm. Simulations are the A0 growing season specification.
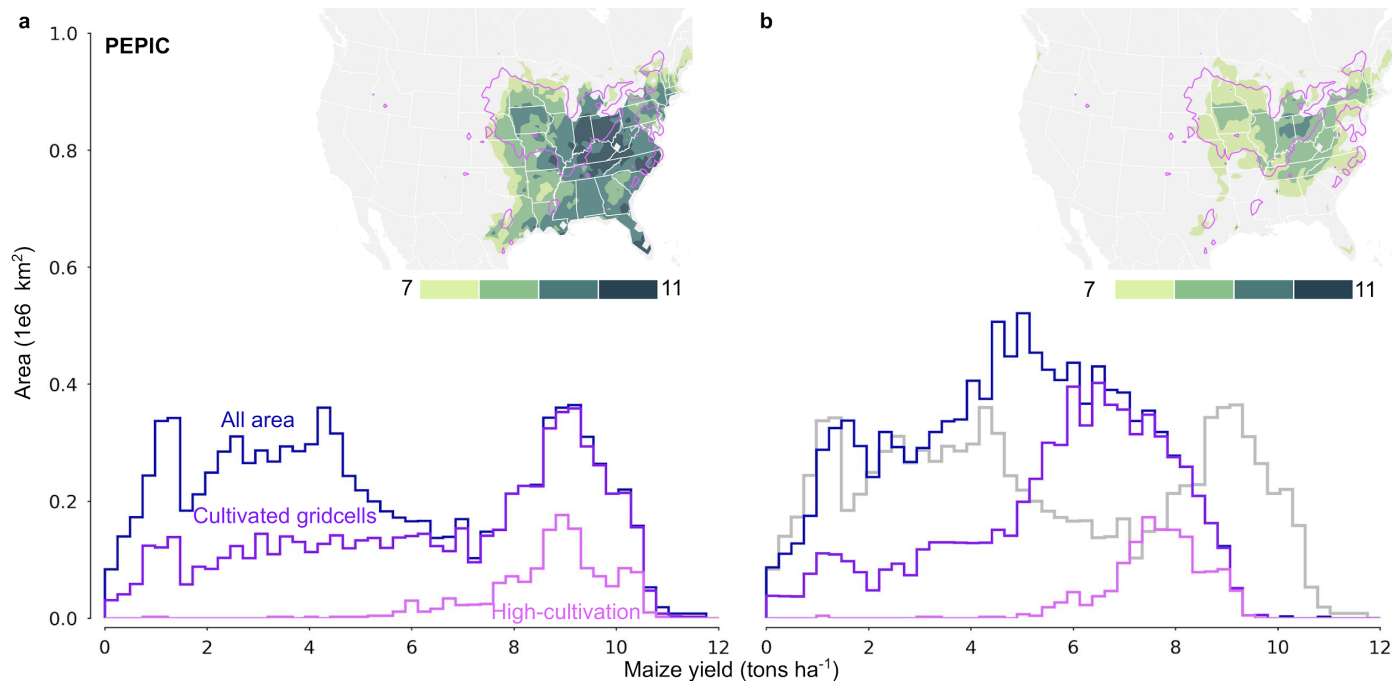
Supplemental Figure S16 | Same convention as main text Figure 2, except now for PROMET. Simulations are the A0 growing season specification.
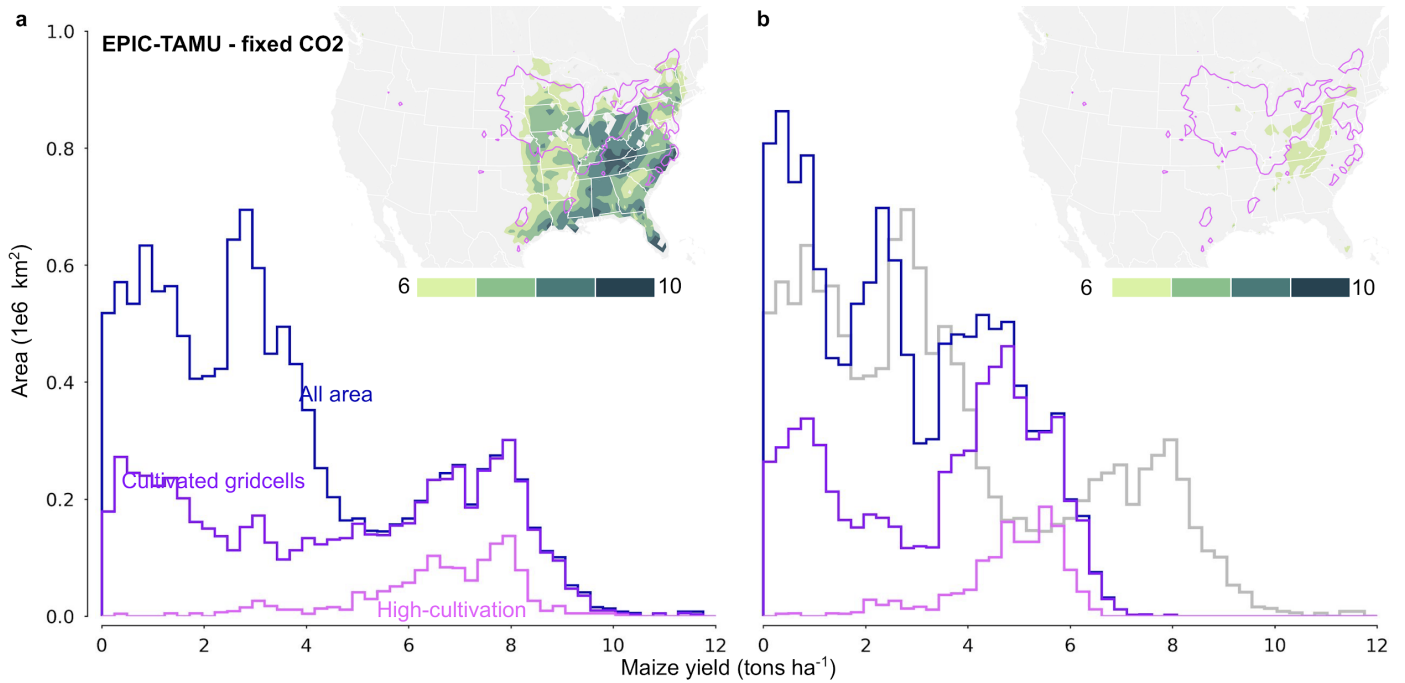

Supplemental Figure S17 | Same convention as main text Figure 2, except now for PROMET with high [CO_2] of 810 ppm. Simulations are the A0 growing season specification.
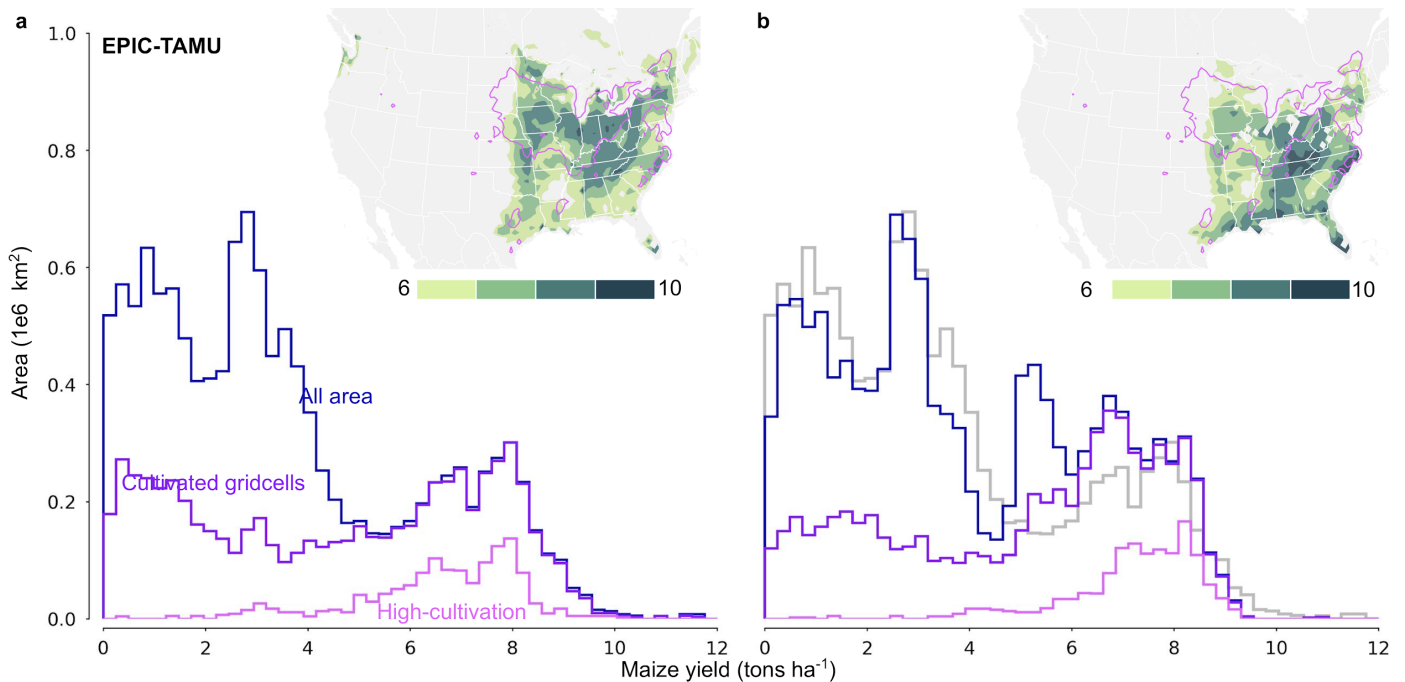
Supplemental Figure S18 | Same convention as main text Figure 2, except now for LPJ-GUESS. Simulations are the A0 growing season specification.
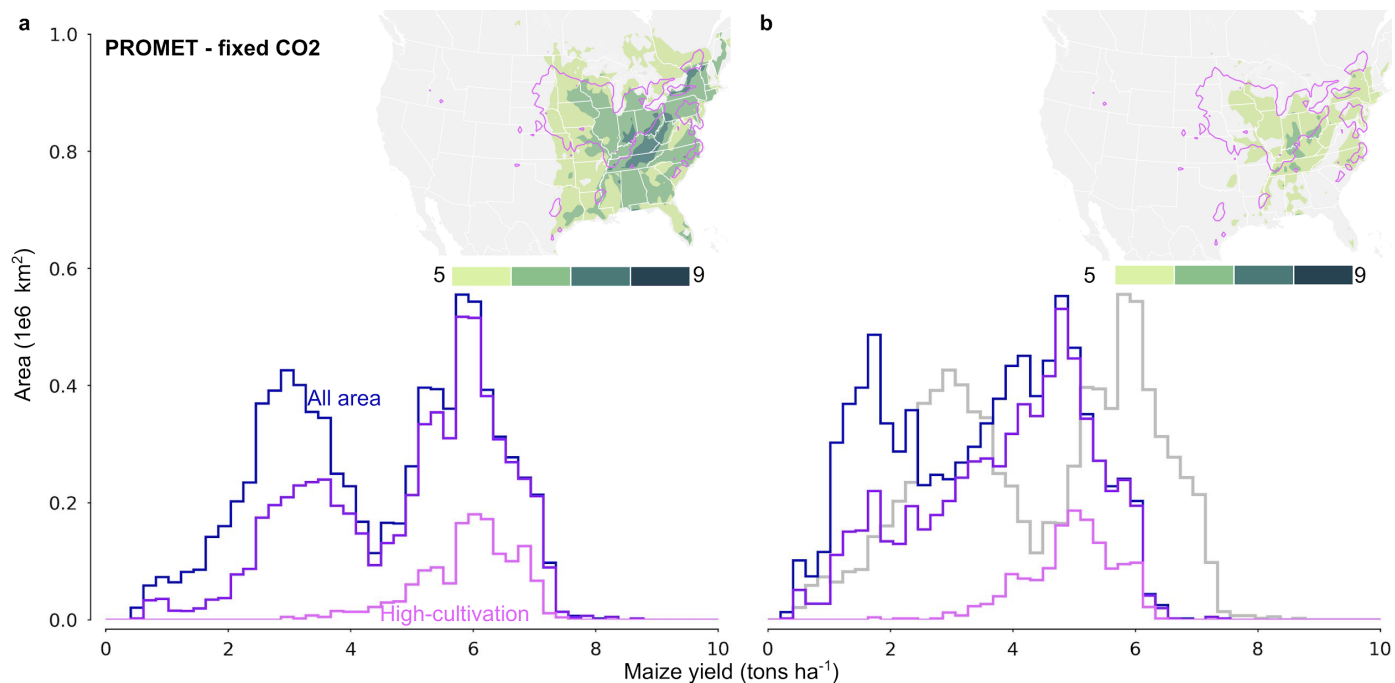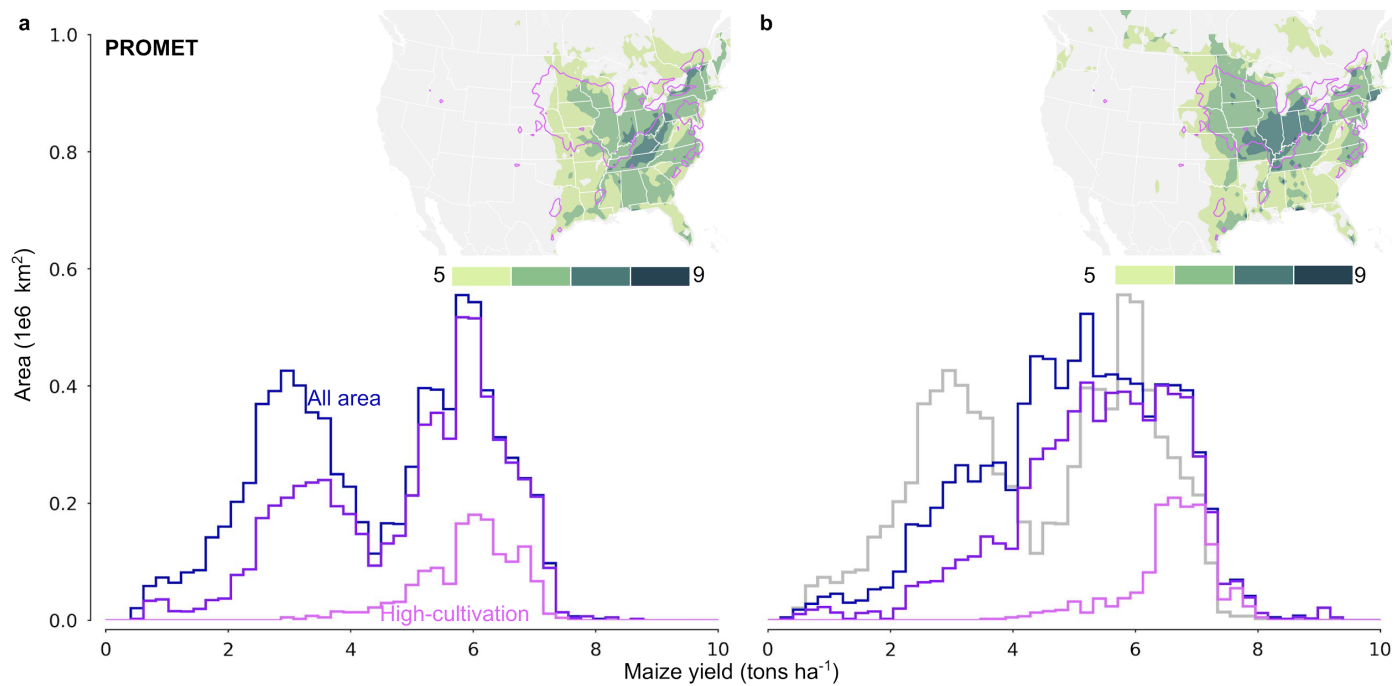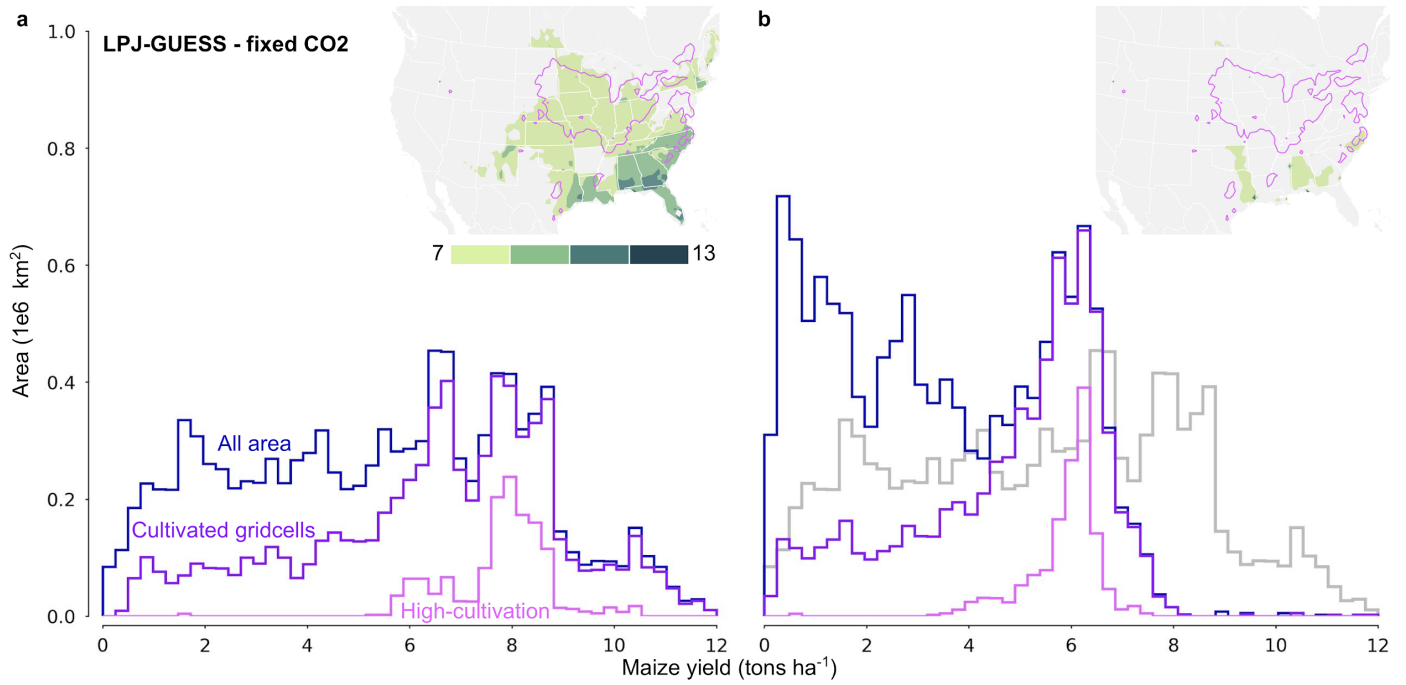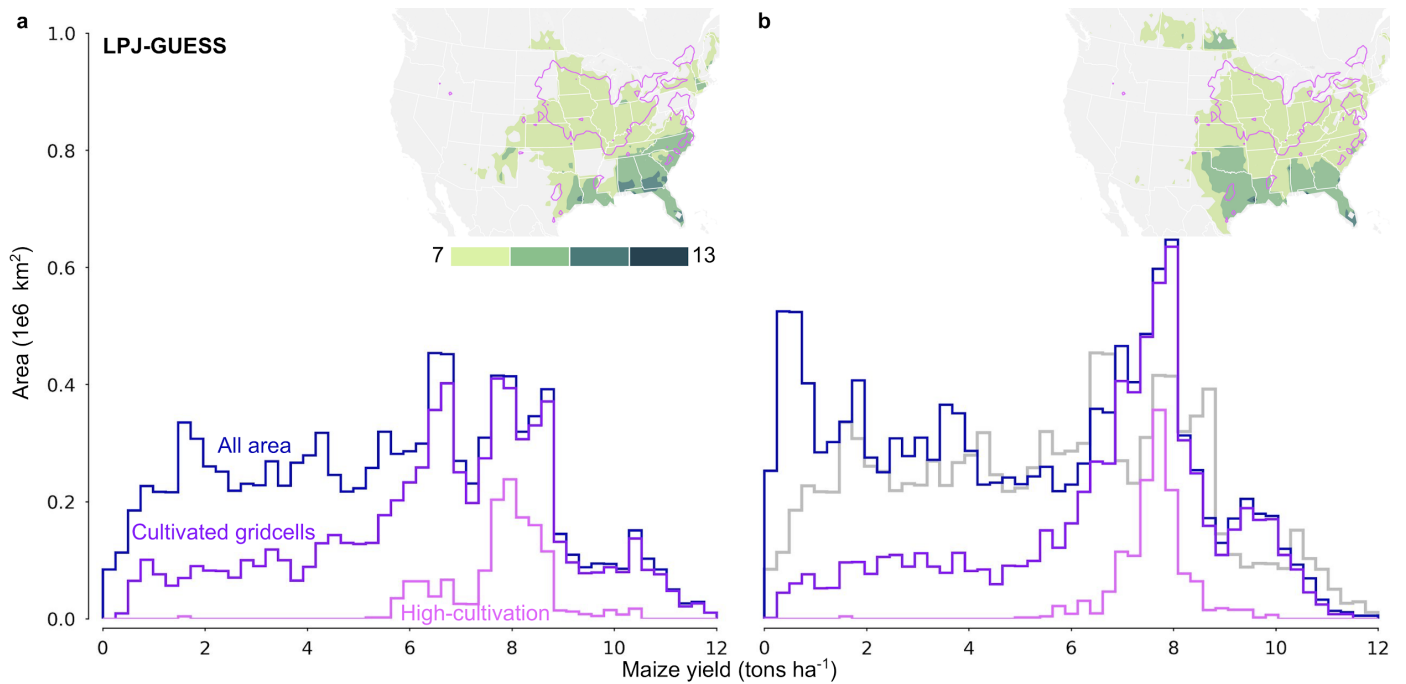

Supplemental Figure S19 | Same convention as main text Figure 2, except now for LPJ-GUESS with high [CO_2] of 810 ppm. Simulations are the A0 growing season specification.
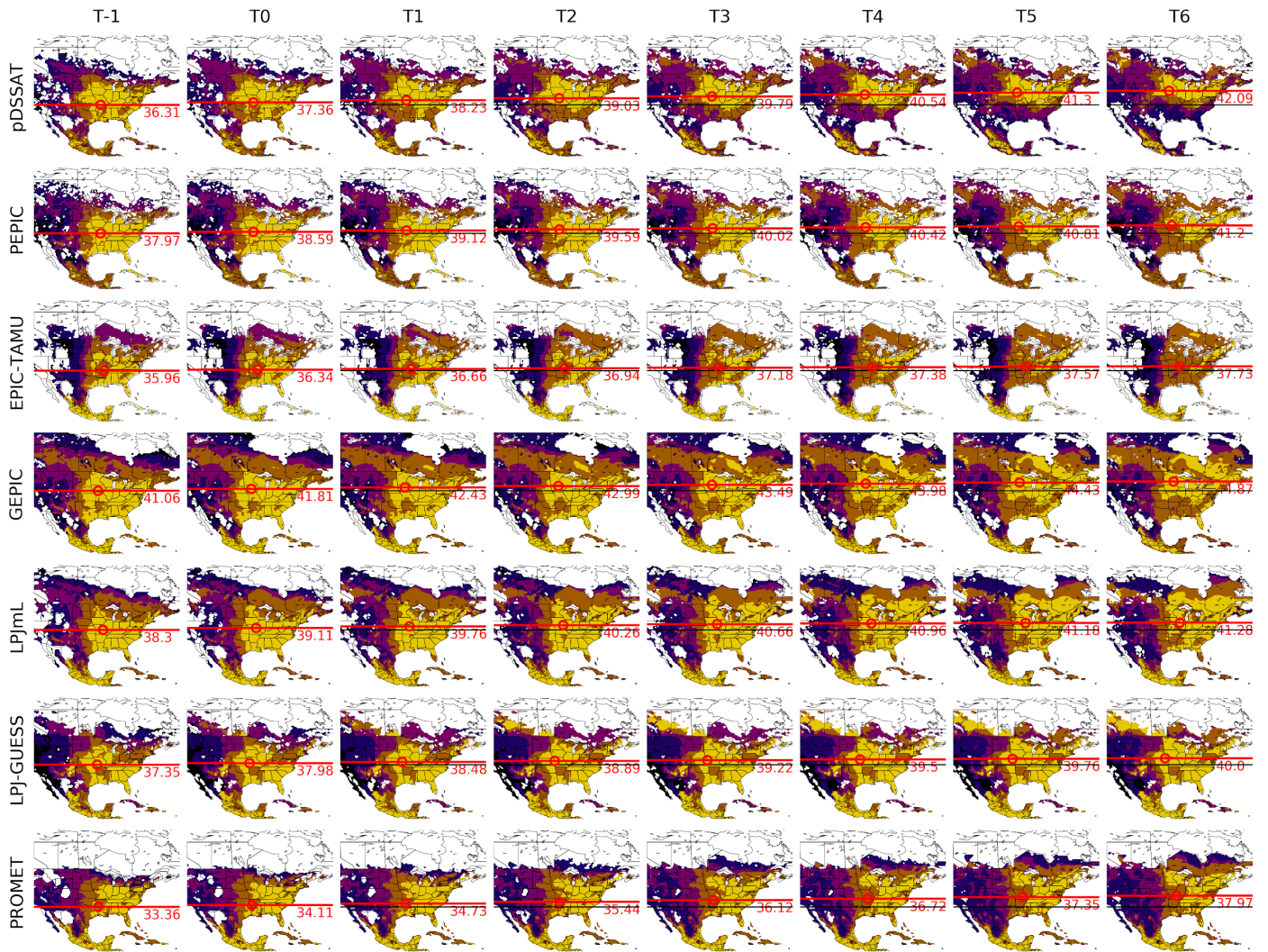
Supplemental Figure S20 | Yield centroid for each model for maize under A0 growing season with [CO_2] of 360 ppm under various degrees of warming (1°C, 2°C, etc). Centroid latitude noted in red. Heatmap shows yield with warmer colors indicating higher yield. Colormaps normalized across models. Simulations are the A0 growing season specification.
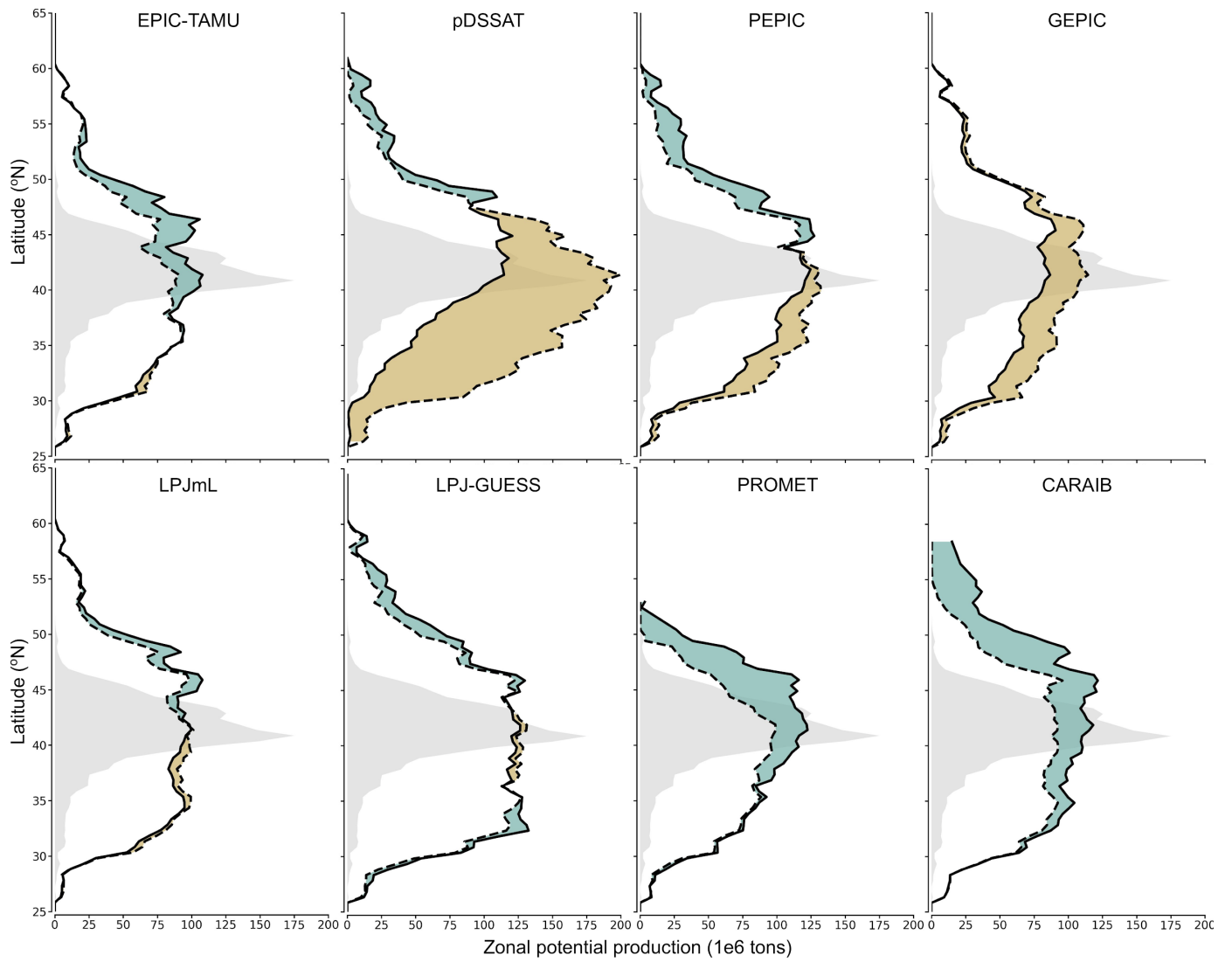
Supplemental Figure S21 | Same convention as above (T+6°C, [CO_2]=810ppm), now for individual models for maize in North America only. Simulations are the A0 growing season specification.
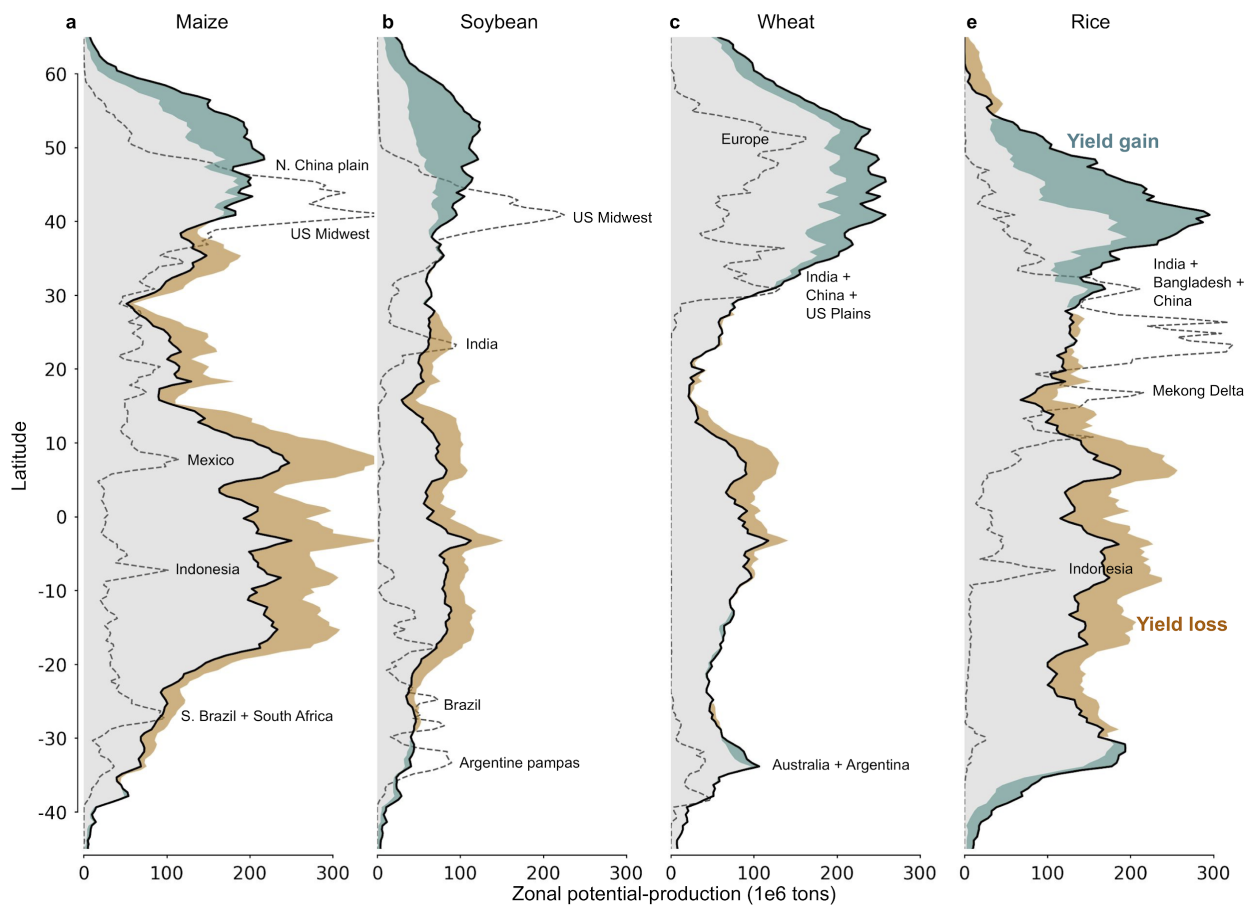
Supplemental Figure S22 | Same convention as main text figure 3, now with simulations at T+6°C and [CO_2] of 810 ppm. Simulations are the A0 growing season specification.
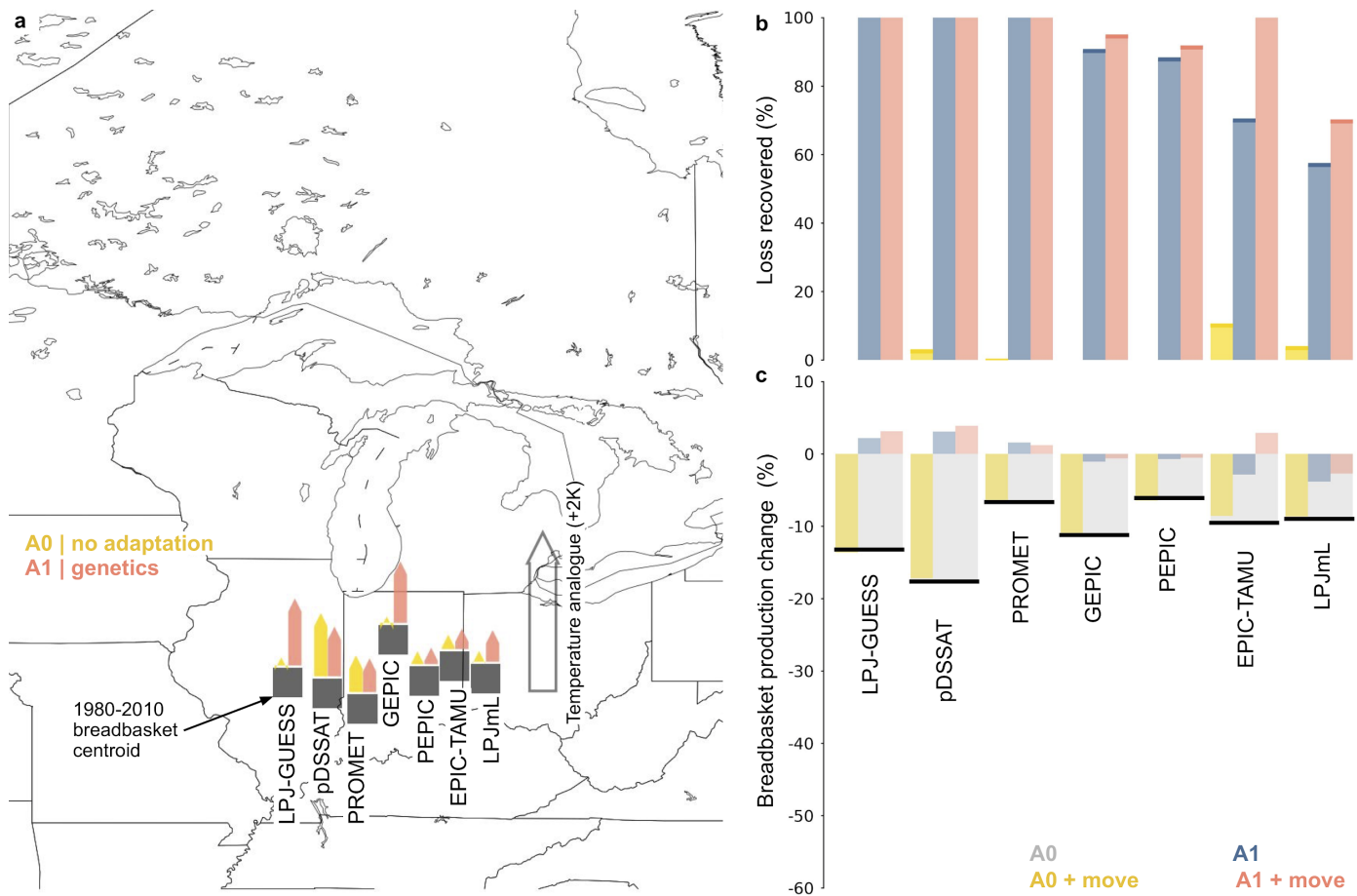
Supplemental Figure S23 | Same convention as main text figure 4, now for 2°C warming. Although effects are smaller, the shifting patterns are the same.
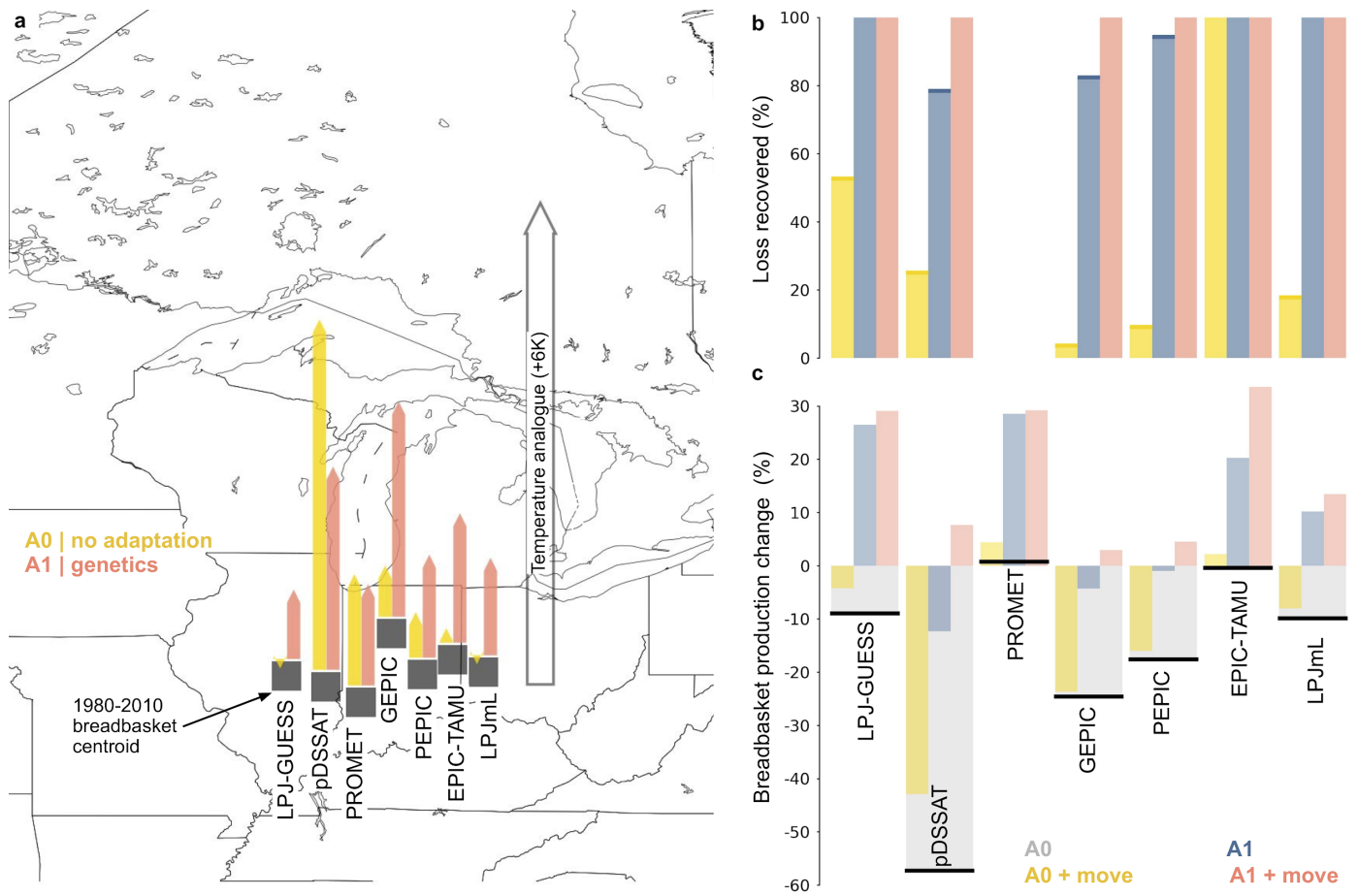
Supplemental Figure S24 | Same convention as main text figure 4, now with [CO_2] at 810 ppm. Shifting patterns are the same as at low [CO_2]. PROMET experiences no losses under 6°C warming and 810 ppm.

Supplemental Table S1 | Growing season changes for the LPJmL simulations driven by the HadGEM climate model. GSL = Growing season length, time between planting and maturity.

Simulation Case	Plant day (doy)	Harvest day (doy)	GSL (days)	Planting advance (% of GSL)	GSL change (%)	T change (K)	Yield change (%)	Poleward shift (km)
Historical (1985-2005)	122	244	122	NA	NA	NA	NA	NA
No adaptation (A0) (2080-2100)	122	206	84	0	-30	6.7	-20	55
Maturity delay (A1) (2080-2100)	122	240	118	0	-3	4.0	-15	610
Planting advance (2080-2100)	101	193	92	+16	-25	1.9	-15	400
Plant + maturity (2080-2100)	101	232	132	+16	+8	2.8	+3	780
Plant + maturity + soils + radiation (2080-2100)	101	232	132	+16	+8	2.3	+8	910
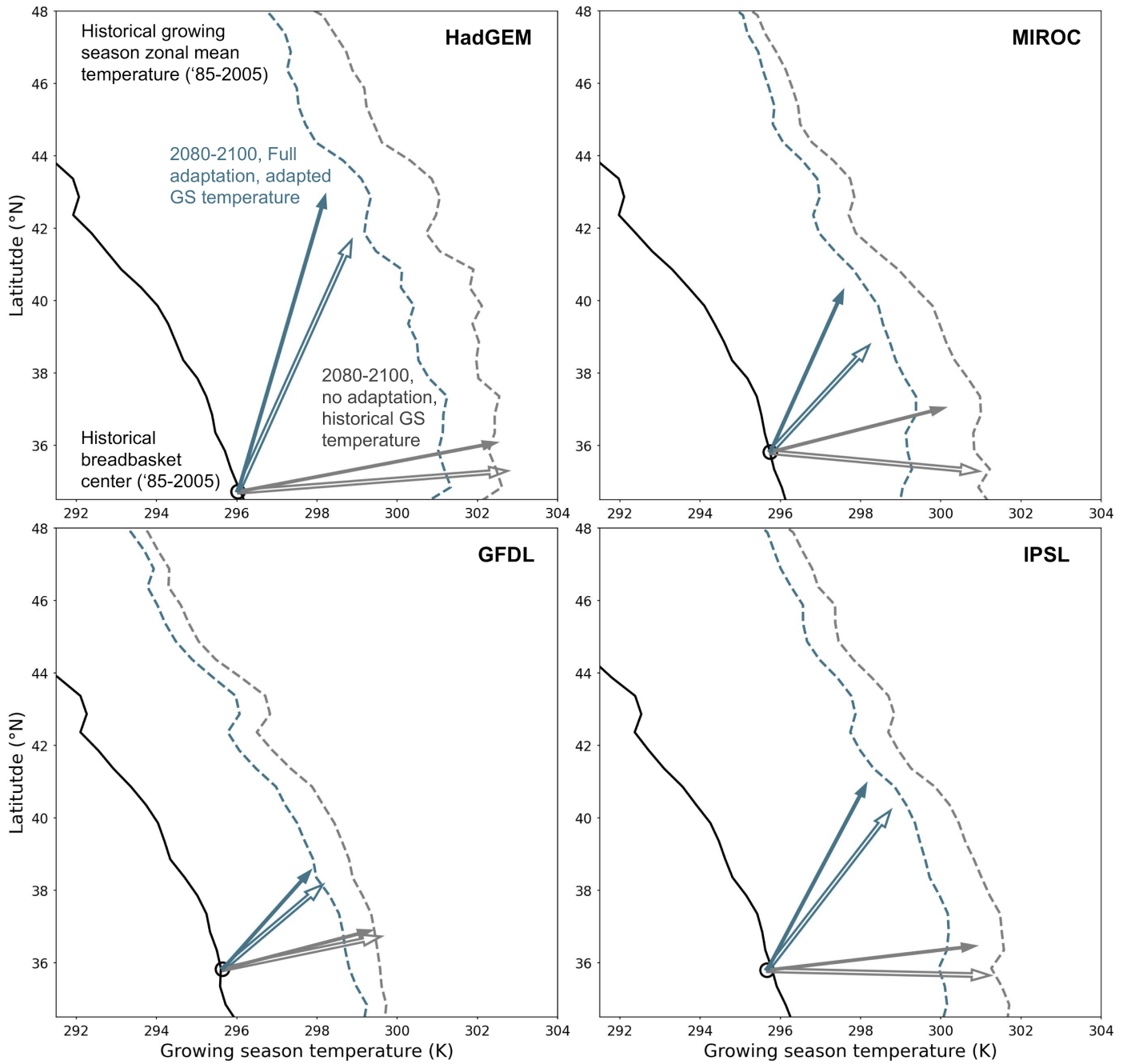
Supplemental Figure S25 | Climate model uncertainty. Same convention as main text figure 5, now for the other climate models. Shown are two separate calculations for mean growing season temperature: one with the planting and harvest date fixed from the historical and one with the actual planting and harvest dates in the model under warming. Trajectories with dynamic [CO_2], according to the RCP, are shown as open arrows.
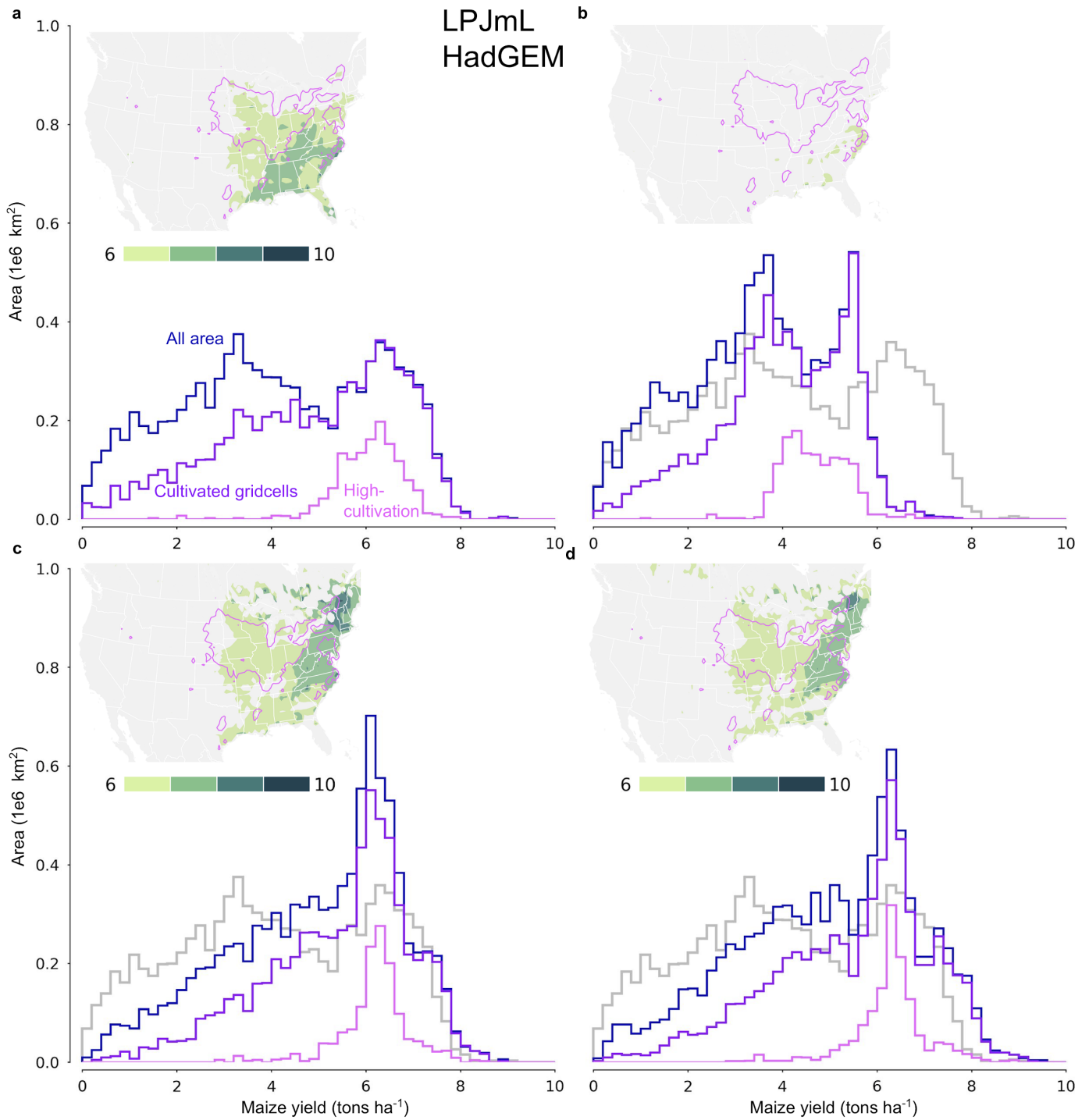
Supplemental Figure S26 | Same convention as main text Figure 2, except now for LPJmL transient runs driven by the HadGEM climate. (a) historical conditions (1985-2005) (b) end of the century (2080-2100) for RCP8.5 (c) end of the century with planting and harvest adaptation (d) end of century with planting and harvest adaptation and Iowa soils and radiation uniformly applied everywhere.
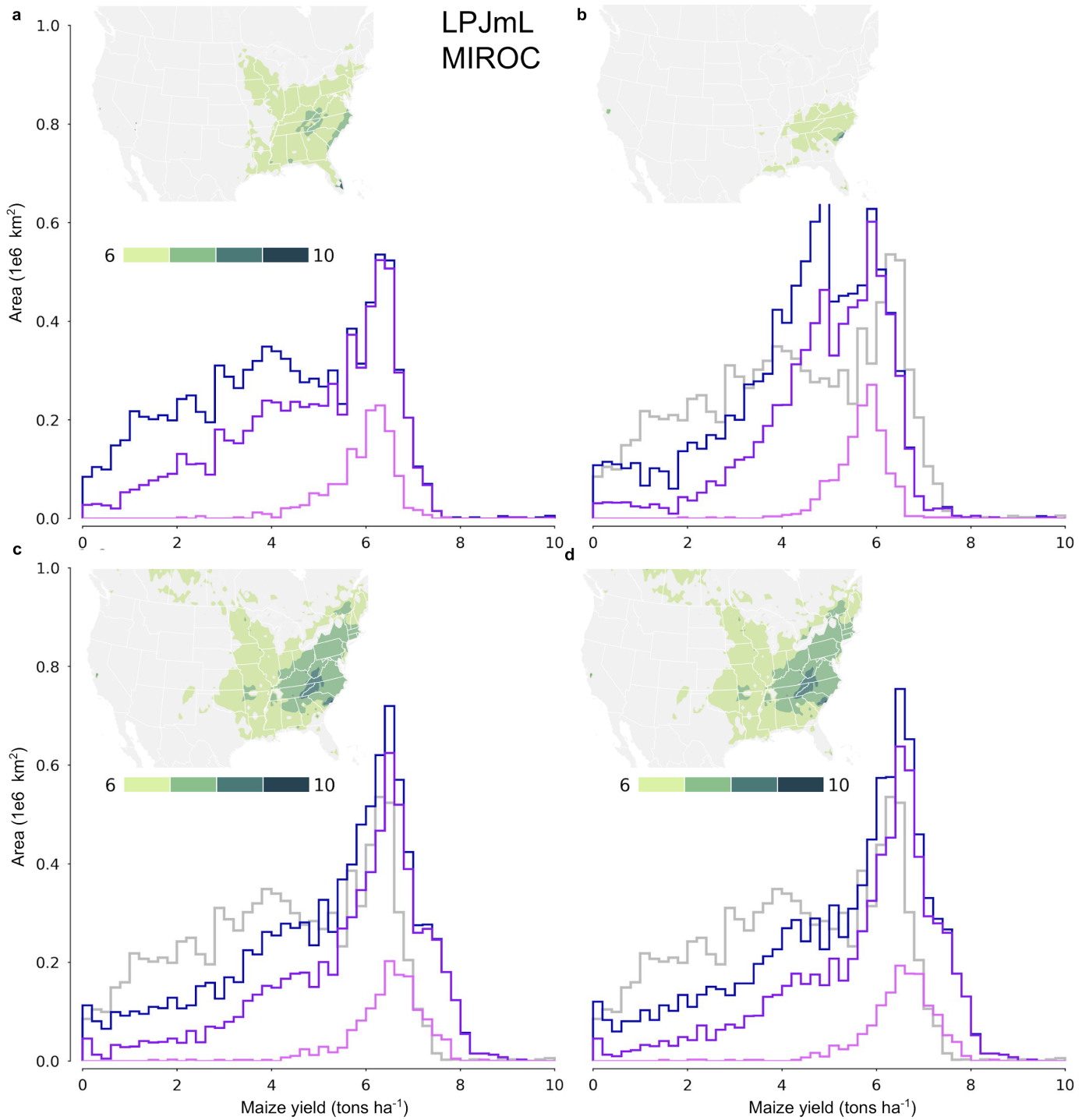
Supplemental Figure S27 | Same convention as above, except now for LPJmL transient runs driven by MIROC5.
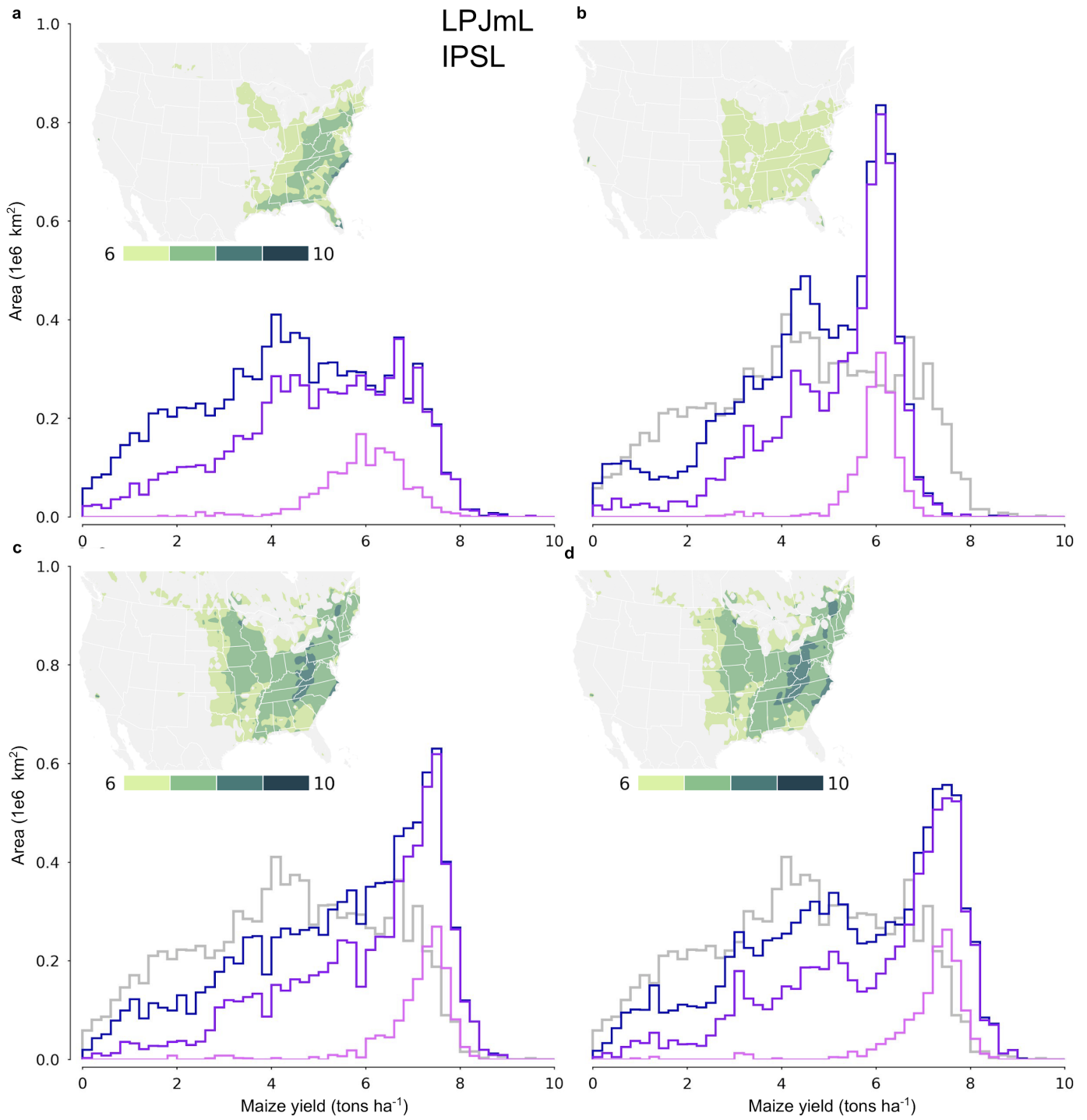
Supplemental Figure S28 | Same convention as above, except now for LPJmL transient runs driven by MIROC5.

Supplemental Figure S29 | Same convention as above, except now for LPJmL transient runs driven by GFDL.

a   North America - **Maize**

2080-2099 (adapted growing season, soils, rad)

2080-2099 (adapted growing season)

2080-2099 (fixed growing season)

1986-2005

90th percentile-yield area →
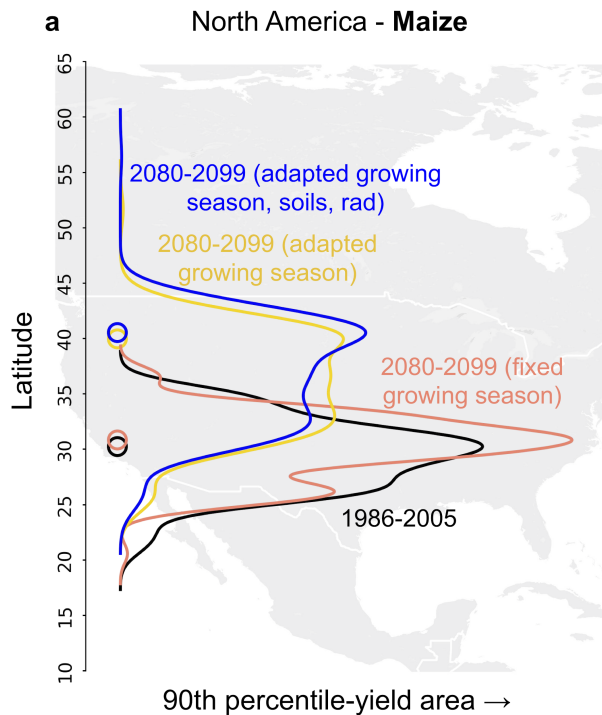
Supplemental Figure S30 | Latitudinal distribution of the highest yielding grid cells in the LPJmL simulation under different growing season adaptation conditions driven by the HADGEM-2 model RCP8.5. Peak la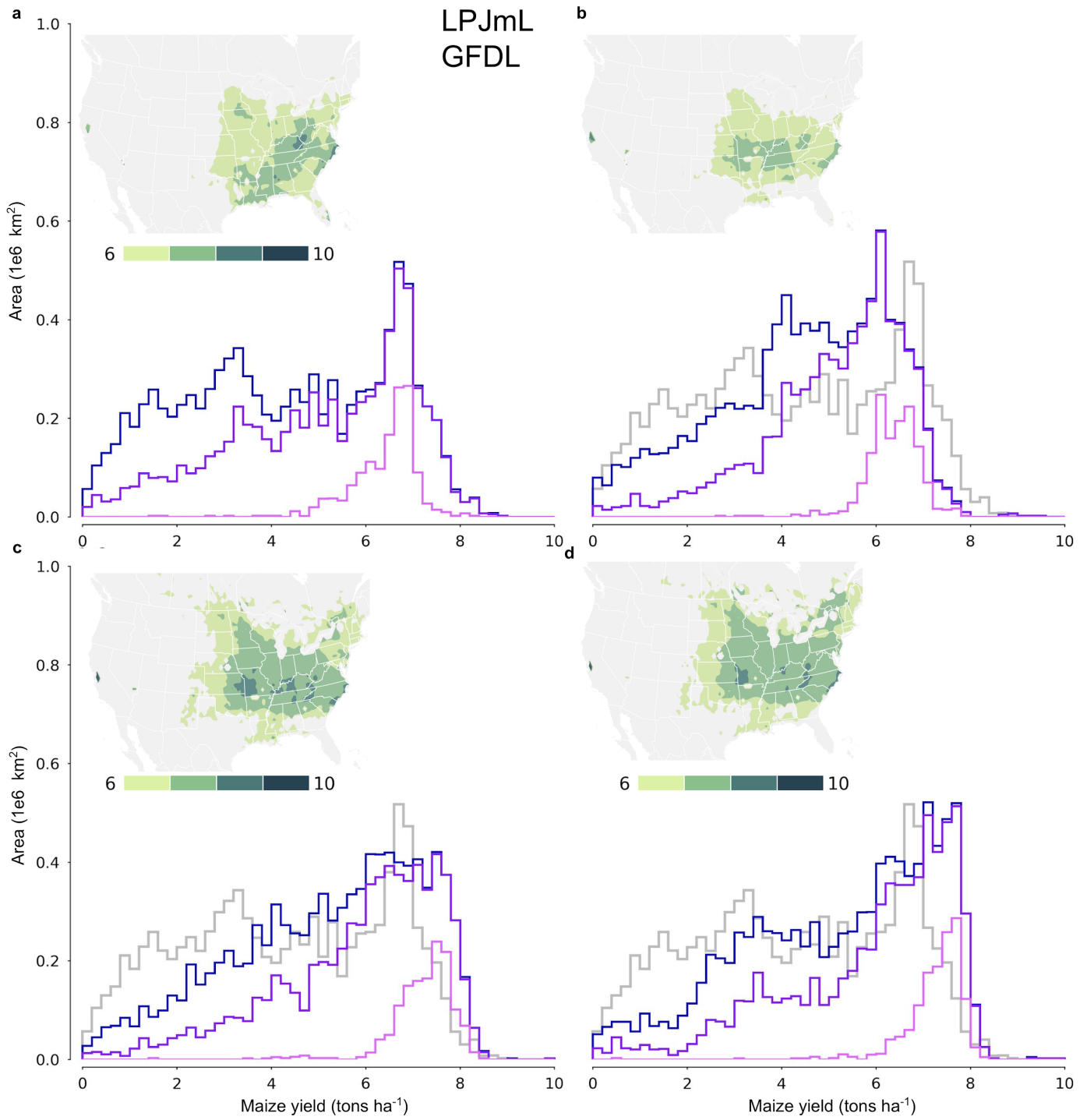titude shown by the open circle. Growing season adaptations are critical to shift the highest-yielding land. Soils and radiation play a lesser role.

Supplemental Table S2 | Figure 6 summary statistics. NA = no adaptation. FA = full adaptation. Shift in land under full adaptation is the percentage of new grid cells which are now in the top 10% of yields at the end of the century.

Breadbasket	Poleward shift, NA (km)	Poleward shift, FA (km)	Shift in land, FA (%)	Production change over current land, NA (%)	Production change FA + shift (%)
North American Maize	55	780	66	-20	+8
South American Soybeans	955	777	46	-23	+26
European Wheat	-290	344	35	-2	+23
East Asian Rice	-122	511	60	-25	+20

Supplemental Table S3 | Percent of area within the breadbasket on the continental scale as shown in Figure 6 in the main text. Some cautions should be taken with interpreting these numbers. The breadbaskets in our analysis are defined as the highest-yielding decile of all grid cells (regionally) -- not by their actual production area and we also do not project future shifts in land-use patterns. How much of a current breadbasket shifts across national borders depends not only on the strength of that shift, but also by the size and geometry of countries, as well as given distortions of yield patterns in GGCMs.

% of area shifting across national borders	No adaptation	Full adaptation
Maize (North america)	0	23
Soybean (South America)	80	67
Wheat (Western Europe)	47	62
Rice (Eastern Asia)	15	30
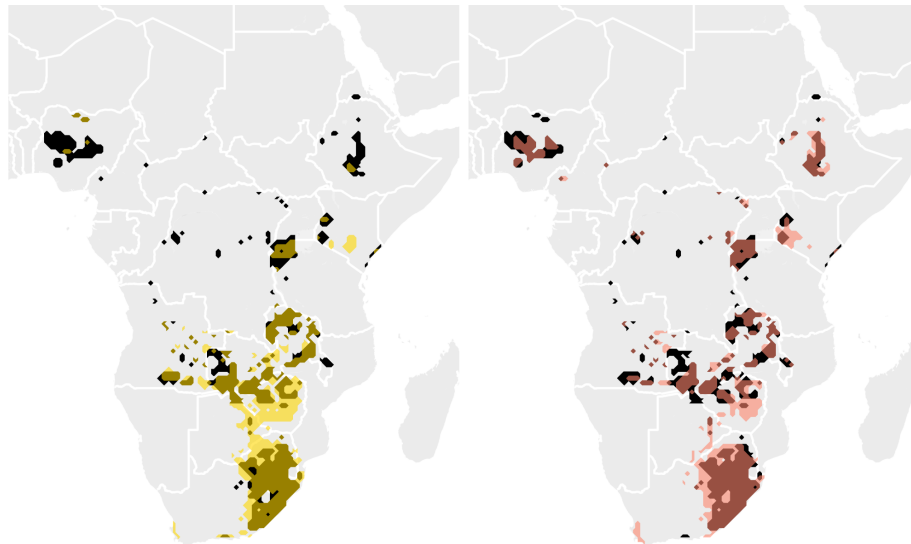
Supplemental Figure S31 | Repeat of Figure 6 in the main text for maize in Africa. Gold = no adaptation. Salmon = full adaptation. The main maize breadbasket in South Africa has nowhere to shift to under warming. Yields in Nigeria and Ethiopia are more resilient with growing season adaptation measures. The simulated maize breadbasket in Africa in less contiguous than other breadbaskets.
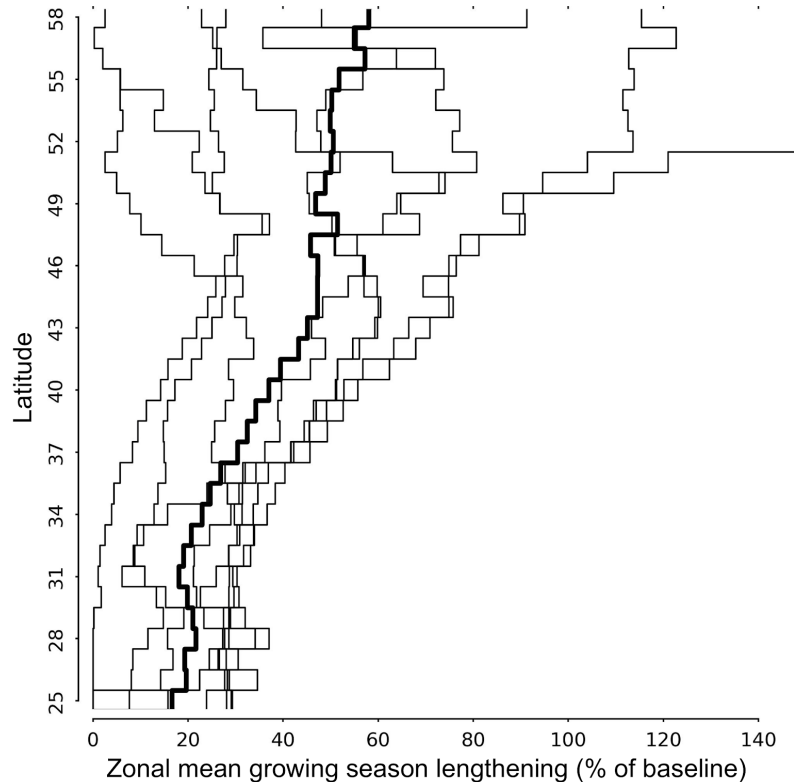
Supplemental Figure S32 | Latitudinal uncertainty in growing seasons changes with warming for maize in North America. Lines indicate the difference in growing season length between A1 and A0 under T+6°C of warming as a percentage of baseline. Zonal mean in North America across agricultural land. Thin gray lines indicated individual models and the thick black line is the ensemble mean. Good model agreement in the mid latitudes where the current breadbasket is centered disappears north of 46 and especially north of 49 latitude.

Supplement References

Frieler K, Lange S, Piontek F, Reyer CPO, Schewe J, Warszawski L, Zhao F, Chini L, Denvil S, Emanuel K, Geiger T, Halladay K, Hurtt G, Mengel M, Murakami D, Ostberg S, Popp A, Riva R, Stevanovic M, Suzuki T, Volkholz J, Burke E, Ciais P, Ebi K, Eddy TD, Elliott J, Galbraith E, Gosling SN, Hattermann F, Hickler T, Hinkel J, Hof C, Huber V, Jägermeyr J, Krysanova V, Marcé R, Müller Schmied H, Mouratiadou I, Pierson D, Tittensor DP, Vautard R, van Vliet M, Biber MF, Betts RA, Bodirsky BL, Deryng D, Frolking S, Jones CD, Lotze HK, Lotze-Campen H, Sahajpal R, Thonicke K, Tian H, and Yamagata Y (2017) Assessing the impacts of 1.5 °C global warming – simulation protocol of the Inter-Sectoral Impact Model Intercomparison Project (ISIMIP2b), Geosci. Model Dev., 10, 4321-4345, doi: 10.5194/gmd-10-4321-2017.

Minoli, S., Müller, C., Elliott, J., Ruane, A. C., Jägermeyr, J., Zabel, F., Dury, M., Folberth, C., François, L., Hank, T., Jacquemin, I., Liu,W., Olin, S. and Pugh, T. A.M. (2019b) Global Response Patterns of Major Rainfed Crops to Adaptation by Maintaining Current Growing Periods and Irrigation. Earth's Future, 7, 1464–1480. URL: https://onlinelibrary.wiley.com/doi/abs/10.1029/2018EF001130

Minoli, S., Egli, D. B., Rolinski, S. and Müller, 458 C. (2019a) Modelling cropping periods of grain crops at the global scale. Global and Planetary Change, 174, 35–46. URL: https://linkinghub.elsevier.com/retrieve/pii/S092181811830362x.

O'Neill, B. C., Tebaldi, C., van Vuuren, D. P., Eyring, V., Friedlingstein, P., Hurtt, G., Knutti, R., Kriegler, E., Lamarque, J.-F., Lowe, J., Meehl, G. A., Moss, R., Riahi, K., and Sanderson, B. M.: The Scenario

Model Intercomparison Project (ScenarioMIP) for CMIP6, Geosci. Model Dev., 9, 3461–3482, https://doi.org/10.5194/gmd-9-3461-2016, 2016.

von Bloh, W., Schapho, S., Müller, C., Rolinski, S., Waha, K. and Zaehle, S. (2018) Implementing the nitrogen cycle into the dynamic global vegetation, hydrology, and crop growth model LPJmL (version 5.0). Geoscientic Model Development, 11,2789–2812. URL: http://dx.doi.org/10.5194/gmd-11-2789-2018.

Waha, K., van Bussel, L. G. J., Müller, C. and Bondeau, A. (2012) Climate-driven simulation of global crop sowing dates: Simulation of global sowing dates. Global Ecology and Biogeography, 21, 247–259. URL: http://dx.doi.org/10.1111/j.1466-8238.2011.00678.x

Portmann, F. T., Siebert, S. and Döll, P. (2010) MIRCA2000-Global monthly irrigated and rainfed crop areas around the year 2000: A new high-resolution data set for agricultural and hydrological modeling: MONTHLY IRRIGATED AND RAINFED CROP AREAS. Global Biogeochemical Cycles, 24, n/a–n/a. URL: http://doi.wiley.com/10.1029/2008GB003435.